JOURNAL OF GEOPHYSICAL RESEARCH, VOL. 92, NO. B10, PAGES 10,443-10,466, SEPTEMBER 10, 1987

U/Pb ZIRCON, STRONTIUM, AND OXYGEN ISOTOPIC AND GEOCHRONOLOGICAL STUDY OF THE SOUTHERNMOST SIERRA NEVADA BATHOLITH, CALIFORNIA

Jason B. Saleeby and David B. Sams

Division of Geological and Planetary Sciences, California Institute of Technology, Pasadena

Ronald W. Kistler

United States Geological Survey, Menlo Park, California

Abstract. The southernmost Sierra Nevada offers a view into the deep levels of the Mesozoic batholithic belt which constitutes much of the range to the north, and represents one of the major tectonic features of western North America. The main crystalline rocks of the study area are (1) the intrusive suite of Bear Valley, a middle Cretaceous tonalite batholith complex with coeval gabbroic intrusives, and (2) the gneiss complex of the Tehachapi Mountains, which consists of Early Cretaceous orthogneiss and subordinate paragneiss, with local domains having granulite facies metamorphic assemblages. The orthogneisses are dominantly tonalitic in composition, with significant layers of granodioritic to granitic and lesser dioritic to gabbroic gneiss. Quartz-rich and psammitic metasedimentary rocks with subordinate marble constitute the main framework assemblage into which the plutonic rocks were emplaced. Field relations demonstrate assimilation of metasedimentary material into the orthogneiss and tonalite batholith magmas, and magma mixing between mafic, tonalitic, and granitic materials. Significant domains of both homogenization and inhomogenization are recognized isotopically within the mixed rocks. U/Pb zircon studies have resolved two major igneous suites and a third suite of postdeformational intrusives, all lying between 90 and 120 Ma. The first suite (gneiss complex of the Tehachapi Mountains) was emplaced at ~115 Ma, and exhibits penetrative high-temperature deformation developed at or near solidus conditions. A number of discordance patterns, along with the physical properties of the zircon, suggest minor inheritance of Proterozoic zircon and limited open system behavior in response to a major 100 Ma plutonic event. The 100±3 Ma intrusive suite of Bear Valley crosscuts the older suite, but also exhibits significant synplutonic deformation. Mainly concordant zircon ages indicate the igneous crystallization age, but some discordances occur due to inheritance or entrainment of Proterozoic zircon. The high-temperature deformation fabrics in these suites and within the metasedimentary framework rocks were crosscut by the granodiorite of Claraville (90 Ma) and pegmatite dikes (~95 Ma). The granodiorite of Claraville shows strong inheritance of Proterozoic zircon and high initial $^{87}Sr/^{86}Sr$ and $\delta^{18}O$. Zircon populations from paragneiss and quartzite samples are dominated by Proterozoic detrital grains. Strontium and oxygen isotopic data on the zircon geochronology sample suite suggest simple two-component mixing of mantle-derived gabbroic to tonalitic magmas with partial to complete melt products from the metasedimentary framework rocks. Sedimentary admixtures for some granitic rocks may be as high as 45%, but for the tonalitic batholithic complex are no higher than about 15%. Modeled values of 10-20% metasediment are typical for the orthogneisses. Initial $^{87}Sr/^{86}Sr$ correlates directly with $\delta^{18}O$, and generally correlates inversely with Sr content. Some subtle complexities in the Sr and O isotopic data suggest the involvement of a third cryptic component. Such a component could be early Phanerozoic ensimatic accretionary terranes that were structurally beneath the observed metasedimentary sequence, or altered oceanic crust and sediments introduced into the mantle magma source area by subduction. One of the initial aims of this study was to seek out remnants of Proterozoic sialic crystalline rocks within the gneiss complex of the Tehachapi Mountains. No such remnants were found, and our studies strongly suggest that sialic components within this link of the Mesozoic batholithic belt were introduced into mantle-derived magmatic systems by anatexis of continent-derived sedimentary rocks.

Paper number 6B6290.
0148-0227/87/006B-6290$05.00

Introduction

Detailed geochronological, petrologic, and geochemical data on the crystalline rocks of the southernmost Sierra Nevada are vital to the understanding of the petrogenetic development of the area, and for regional tectonic analysis. Recent work [Sams and Saleeby, 1987; Ross, 1985, 1987; Sams et al., 1983] shows Sierran batholithic plutons grading into a gneiss complex in the Tehachapi Mountains. Work by Sharry [1981] emphasized the presence of pyroxene and garnet in some of the gneiss units, and their resemblance to granulites. He speculated a deep-seated metamorphic origin for the "granulites", and their subsequent rapid Late Cretaceous uplift. Work by Saleeby et al. [1986], Elan [1985], and Saleeby [1981] in the south-central Sierra Nevada suggests that the depth of exposure of the batholith increases southward from mesozonal levels (~10 km depth) in the Lake Isabella area to catazonal levels (20-25 km) in the gneiss complex. U/Pb age dating on plutonic rocks, and on "granulitic" and amphibolitic gneiss bodies, exhibits zircon populations with systematics suggestive of Cretaceous igneous crystallization [Sams et al., 1983; this study]. The zircon systematics and physical characteristics are for the most part similar to

those from mesozonal batholithic plutons of the central Sierra Nevada [Chen and Moore, 1982; Saleeby and Sharp, 1980].

Zircon geochronological studies were initiated in 1981 in order to investigate two major topics: (1) the possible existence of remnants of Proterozoic sialic basement within the southernmost Sierra Nevada crystalline framework, and (2) structural and petrogenetic relations between the composite batholith and gneissic rocks reported in reconnaissance studies by Ross [1980]. Geochemical studies by DePaolo [1981] and Kistler and Peterman [1973, 1978] indicate that Proterozoic sialic material is a major component in the materials contributed to the Sierran batholithic rocks, and that the southern and central part of the batholith consists of homogenized Proterozoic sialic material and mantle-derived island arc material. The question as to whether the Proterozoic components were contributed to the mixing reservoirs as crystalline rocks, or as sediments derived from such crystalline rocks, carries important petrogenetic and tectonic implications. Strontium and oxygen isotopic studies were conducted on the zircon sample suite in order to explore this question in light of detailed zircon studies.

The age and structural configuration of the southernmost Sierra crystalline rocks carry important regional implications. One of the outstanding tectonic features of southern California is a family of highly tectonitic schists (Pelona, Rand, and Orocopia schists) that lie tectonically beneath crystalline rocks of both Proterozoic and Mesozoic age [Haxel and Dillon, 1978; Ehlig, 1981; Silver et al., 1984]. Such schists may tectonically underlie the entire southern California region [Yeats, 1981]. The remnants of a thrust contact between the gneiss complex of the Tehachapi Mountains and lower plate Rand Schist preserved along the northern edge of the Garlock fault zone (Figure 2) were mapped by Sharry [1981]. This structural relation, in conjunction with the demonstration of structural continuity between Sierran batholithic rocks and the gneiss complex of the Tehachapi Mountains [Sams and Saleeby, 1987; this study], reveals the only known pre-Neogene contact relations between Sierran and southern Californian basement regimes. Thus, the study area constitutes a strategic link between northern and southern California tectonic regimes, whose interrelations are poorly understood.

The purpose of this work is to present the isotopic and geochronological data and to summarize the petrogenetic and tectonic implications of the data. Detailed discussions of the petrology and tectonics of the study area are presented by Sams and Saleeby [1987], Sams [1986], Ross [1980, 1983b, 1987], and Sharry [1981]. A brief overview of the field and petrographic data is presented first as a geological framework for the isotopic and geochronological data.

Geological Summary

The study area encompasses the southern end of the Sierra Nevada, which has a regional NNW trend that swings around to an ENE orientation in the Tehachapi Mountains (the Sierran "tail" of Ross [1980, 1987]). The southernmost Sierra Nevada

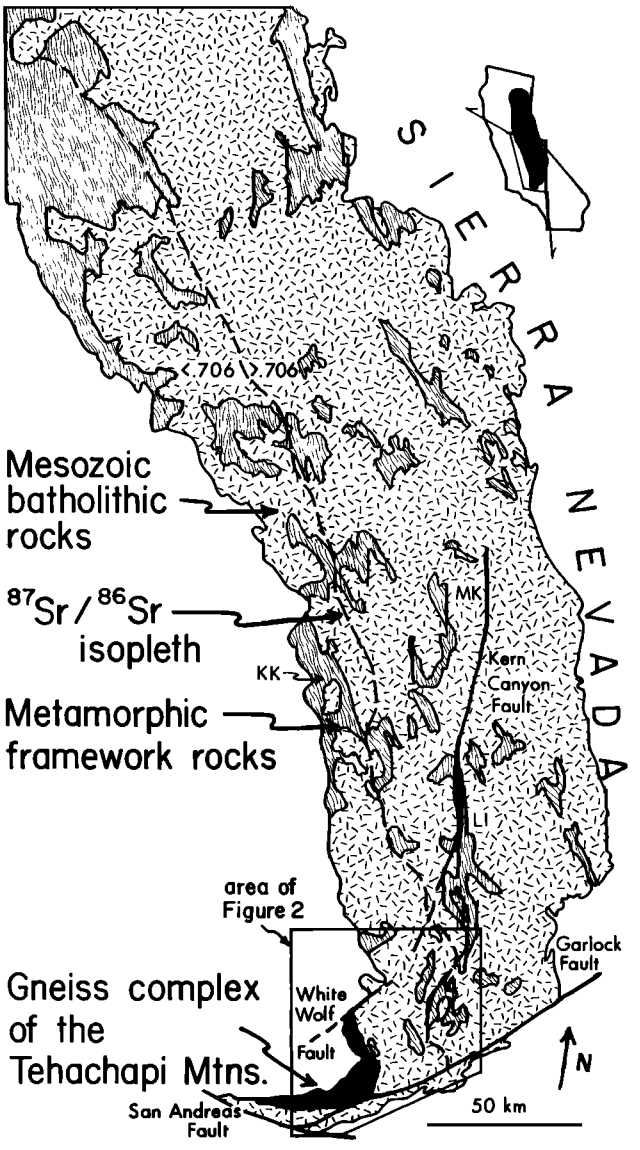

Fig. 1. Map showing location of study area and major tectonic and geographic features referred to in text. Initial $^{87}Sr/^{86}Sr$ on Sierra Nevada batholithic rocks after Kistler and Peterman [1973, 1978]. KK, Kings-Kaweah ophiolite belt; MK, Mineral King; LI, Lake Isabella.

crystalline terrane (Figures 1 and 2) is characterized by thin metamorphic septa and voluminous Cretaceous plutonic rocks [Ross, 1980, 1987; Sams and Saleeby, 1987; Saleeby et al., 1978; Sams et al., 1983]. Prevailing structures within the crystalline rocks are foliation surfaces and lithologic contacts, which are steeply dipping, with an overall northwest trend, except for the southernmost "tail" of the Sierras, where northeast and east trends are common. The crystalline rocks are overlain unconformably by middle to upper Eocene marine strata [Nilsen and Clarke, 1975; Harris, 1954] and by Quaternary deposits.

Typical Sierran batholithic rocks can be traced southward to the vicinity of Tejon Creek, where they grade into the gneiss complex of the Tehachapi Mountains (Figure 2). Metasedimentary

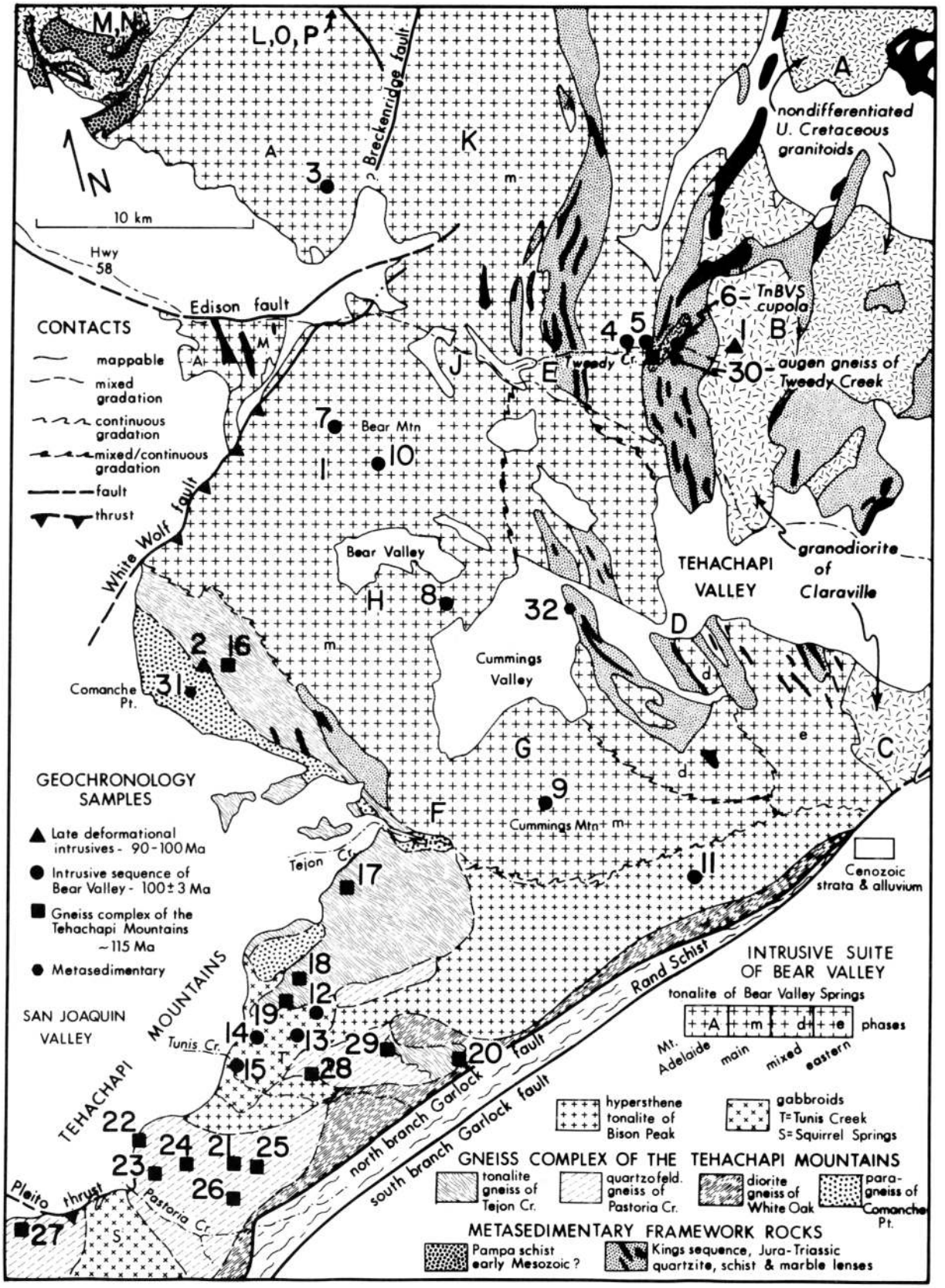

Fig. 2. Generalized geologic map showing crystalline rocks of the southernmost Sierra Nevada and locations of isotopic age samples (numbers are zircon, Sr, and O samples; letters are Sr samples). Lithologic units are taken primarily from Sams [1986] and Ross [1980] with modifications after Sharry [1981] and Ross [1987].

septa within the batholith, whose structures parallel those in the batholith, also continue to Tejon Creek, where they become migmatitic. South of Tejon Creek, the crystalline rocks consist almost entirely of orthogneiss, granofels, and migmatitic paragneiss.

Batholithic rocks and orthogneisses of the study area are divided into two major suites based on age, intrusive chronology, and deformational fabrics. The first suite, dated at ~115 Ma, includes the orthogneisses from the gneiss complex of the Tehachapi Mountains. The second suite, 100±3 Ma, consists of the intrusive suite of Bear Valley. A third group of 90 and ~95 Ma late or postdeformational intrusive rocks was also studied in order to place absolute age constraints on the near-penetrative ductile deformation observed in the two major suites. The preintrusive framework rocks observed for the major suites are totally metasedimentary.

The Metasedimentary Framework Rocks

The Kings sequence represents the metamorphic framework into which the intrusive rocks of the study area were emplaced. It forms a series of discontinuous septa from Tejon Creek to areas north of the study area. Similar rocks have been traced for over 200 km northwards, and constitute one of the main framework assemblages for the composite Sierra Nevada batholith [Saleeby et al., 1978]. In the region of the study area the septa consist of lenses of impure quartzite, marble, and calc-silicate rock, encased within a quartz-mica schist matrix. Psammitic to quartzofeldspathic granofels and gneiss are locally present, especially in the vicinity of Cummings Valley. Recognizable Kings sequence rocks occur within the gneiss complex as 10-100 m lenses of coarsely recrystallized marble and quartzite. The migmatitic paragneiss of Comanche Point is interpreted as a Kings sequence psammite.

The Kings sequence is primarily an early Mesozoic continent-derived clastic sedimentary sequence. Basement for the sequence is unknown, although Saleeby et al. [1978] hypothesized mainly a Proterozoic North American basement on the basis of geographic location to the high side of the initial $^{87}Sr/^{86}Sr = 0.706$ isopleth within the batholith. Such an analysis is brought into question by the data and conclusions presented below. The 1978 publication also noted, however, that a western facies of the sequence laps depositionally onto the Paleozoic Kings-Kaweah ophiolite belt (Figure 1). Rocks forming the septa of Pampa Schist in the northwest corner of the study area (Figure 2) are similar to early Mesozoic basinal strata which lie on the ophiolite belt and contain interbeds and slideblocks of western Kings sequence strata. Ophiolitic basement cores have been recovered from the subsurface immediately west of the Pampa Schist septa [Sams and Saleeby, 1987]. It is thus suggested that the general stratigraphic framework observed in the Kings-Kaweah region extended into the study area prior to emplacement of the Cretaceous intrusive rocks.

The Gneiss Complex of the Tehachapi Mountains

The gneiss complex of the Tehachapi Mountains is defined [Sams and Saleeby, 1987] as a collection of felsic to mafic orthogneisses that have U/Pb ages of mainly 110 to 120 Ma, and contain pervasive high-temperature deformational fabrics exhibited by the transposition of internal contacts, and gneissic banding. Subordinate mappable paragneiss bodies are also included in the complex. Map units that have been distinguished on the basis of field, petrographic, and age criteria include the tonalite gneiss of Tejon Creek, the quartzofeldspathic gneiss of Pastoria Creek, the paragneiss of Comanche Point, the diorite gneiss of White Oak, and the augen gneiss of Tweedy Creek. Their mutual contacts are typically obscure, but where observed, are generally gradational. Sharp, intrusive contacts are infrequent and are restricted primarily to the Bison Peak and Tunis Creek units of the intrusive suite of Bear Valley as well as small gabbroic to wehrlitic pods grouped into the gneiss units.

The tonalite gneiss of Tejon Creek is a biotite hornblende tonalite gneiss, with K-feldspar, and rare clinopyroxene or orthopyroxene. It is pervasively foliated but only weakly gneissose; it retains a clear igneous fabric. The paragneiss of Comanche Point consists of quartzofeldspathic leucosomes and biotite-rich layers that alternate on a centimeter scale, as well as subordinate scapolite-bearing calc-silicate lenses; it is pervasively migmatitic. The Tejon Creek tonalite intrudes and is observed to have assimilated part of the paragneiss. Muscovite and garnet are found in the tonalite near the contact with the paragneiss along with local restite. The Pastoria Creek unit is a heterogeneous collection of gneisses that occur as distinct 1-10 km bodies throughout the Tehachapi Mountains. Compositions range from diorite-tonalite banded gneiss to granitic banded and augen gneiss. The Pastoria Creek unit is distinct from the other gneiss units on the basis of a greater heterogeneity and wider compositional range at mesoscales and map scales. Local pods of granulite facies metasedimentary gneiss and granofels occur within the Pastoria Creek unit. Gabbroic to wehrlitic lenses of up to 100 m in length are dispersed throughout all the orthogneiss units of the complex. The White Oak unit is a pervasively sheared biotite hornblende diorite gneiss with lesser quartz diorite. High-temperature deformation fabrics are commonly overprinted by lower-temperature brittle deformation and retrograde minerals; for this reason we did not sample this unit in this study. Late-stage deformation in this unit is related to the tectonic contact with the Rand Schist.

The augen gneiss of Tweedy Creek is separated from the main gneiss complex by intrusive rocks of the Bear Valley suite. It is a highly tectonitic orthogneiss that both crosscuts and shares the deformational fabrics of its Kings sequence host. Although the augen gneiss is physically removed from the main complex, it is similar to felsic augen varieties of the Pastoria Creek unit, and yields a similar zircon age. The Tweedy Creek unit was investigated as part of the search for Proterozoic crystalline basement.

The Intrusive Suite of Bear Valley

The intrusive suite of Bear Valley consists of the tonalite of Mount Adelaide, the tonalite of Bear Valley Springs, the hypersthene tonalite of

Bison Peak, and the gabbroids of Tunis Creek and Squirrel Spring. The members of this suite have ages of 100±3 Ma and are typical of the western margin of the Cretaceous Sierra Nevada batholith. The tonalite of Bear Valley Springs is a batholith-scale pluton, with its southern margin gradational into the Bison Peak unit. The western margin of the batholith is an apparent gradation zone with the tonalite gneiss of Tejon Creek. Structures and foliations within the Bison Peak and the tonalite gneiss parallel those within the batholith. The tonalite batholith extends at least 30 km north of the study area.

The batholith is a composite body of mainly biotite hornblende tonalite. It retains an igneous texture throughout, although much of it has been ductilely deformed, resulting in a steep foliation oriented subparallel to its margins. Hypersthene is present in the southern parts of the batholith, while mafic inclusions and schlieren are common throughout. Such inclusions and schlieren for the most part represent synplutonic injections of gabbroic to quartz dioritic magma batches [Sams and Saleeby, 1987]. The batholith has been divided into four phases on the basis of field, petrographic, and geochemical data. The main, mixed, and eastern border phases (Figure 2) are intergradational and constitute the major part of the batholith in the study area. They have subequal hornblende to biotite ratios, a pervasive foliation, and significant amounts of mafic inclusions. The main and eastern border phases are moderately uniform in character, with the eastern phase exhibiting considerable deformation related to differential movement with respect to the adjacent metasedimentary framework. The eastern phase may have included distinct magma batches 1 to 2 m.y. younger than the main phase. Possible internal contacts are obscured by deformation. The mixed phase can be distinguished from the main and eastern phases by its higher concentrations of mafic inclusions and schlieren and the occurrence of major zones of hypersthene-bearing tonalite and local leucotonalite to granodiorite. The mixed phase is localized along a highly dismembered framework septum and grades into the main and eastern border phases by a decrease in mafic inclusions, hypersthene-bearing rock, and leucotonalite. The northern Mount Adelaide phase is a nondeformed biotite tonalite which clearly crosscuts the main phase.

The Bison Peak, Tunis Creek, and Squirrel Spring units are partially to completely encased within the gneiss complex. The Bison Peak unit is a hypersthene-bearing biotite hornblende tonalite having local intrusive contacts preserved with rocks of the gneiss complex. The gabbroids of Tunis Creek and Squirrel Spring are ovoid bodies with relatively little internal ductile deformation. Compositions are chiefly gabbroic but range from diorite to melagabbro, anorthosite, and wehrlite. Hornblende is the dominant mafic phase, although olivine and pyroxene are widespread. Cumulate textures and structures are common, and for the most part the gabbroids are typical of the western Sierra Nevada batholith calcic gabbro suite [Saleeby and Sharp, 1980]. A noteworthy aspect of the Tehachapi gabbroids is the local presence of subsolidus (disequilibrium) almandine-rich garnet [Sams and Saleeby, 1987].

The intrusive suite of Bear Valley locally crosscuts the deformational fabric of the gneiss complex. The intrusive suite does contain planar ductile deformation fabrics developed under solidus to hot subsolidus conditions within the tonalitic members, whereas the gabbroids contain igneous-flow and compositional layering structures. The younger suite can be distinguished from the gneiss complex on the basis of local intrusive relations and a general lack of gneissic banding. The major magmatic event represented by the intrusive suite is interpreted as the culmination of the high-temperature environment, represented in part by the gneiss complex. Recrystallization and ductile deformation fabrics are present in the intrusive suite of Bear Valley but are less pervasive and less intense as compared to those of the gneiss complex. Retrograde reactions of olivine to orthopyroxene and pyroxene to amphibole are common in both suites, while evidence for prograde reactions is virtually absent, except within the metasedimentary framework rocks.

Tectonic Setting

Early Cretaceous batholithic rocks of the western Sierra Nevada and eastern Great Valley subsurface represent magmatism related to the earlier phases of Franciscan subduction [Saleeby, 1981]. The study area is of special interest in this regard because it exposes the deepest known level of the subduction-related magmatic arc. Recent work on the crystalline rocks of the study area suggests a considerably deeper level of exposure of the Sierran composite batholith and its metamorphic framework as compared to areas to the north [Ross, 1985, 1987; Sharry, 1981; Sams, 1986; Sams et al., 1983; Saleeby et al., 1986]. The transition from the mesozonal composite batholith to the deep-level terrane occurs over a distance greater than 100 km. Throughout the transition zone and within the deep-level terrane, batholithic and regional metamorphic processes cannot be clearly separated. Petrologic and field data leading to the interpretation of a deep-crustal origin for the study area consist of (1) geobarometric studies suggesting regional peak metamorphism at perhaps as high as 8 kbar [Sharry, 1981]; (2) magmatic epidote-bearing tonalites within the Pastoria Creek unit [Sams, 1986; Zen and Hammarstrom, 1984; Zen, 1985]; (3) local hot subsolidus, autometamorphic garnet growth within gabbroidal to tonalitic rocks, where the garnet-in reaction curve is suggested to occur at 6-8 kbar [Sams, 1986; Green, 1982]; and (4) local occurrence of high $\delta^{18}O$, graphite-bearing metasedimentary granulites [Ross, 1983b, 1987]. The widespread occurrence of migmatitic and strongly gneissose rocks is also consistent with a deep-seated origin for the study area. Field relations and zircon data show that such deep-seated rocks not only are in structural continuity with typical Sierran batholithic rocks, but are also similar in igneous age to the western and axial parts of the batholith.

The gneiss complex and the intrusive suite of Bear Valley exhibit near-penetrative ductile deformation developed under solidus and hot subsolidus conditions. Such deformation is interpreted as an inherent feature of the deep-seated conditions within the magmatic arc [Saleeby et al., 1986; Sams and Saleeby, 1987]. Direct evi-

TABLE 1. Zircon Geochronology Sample Locations, Interpreted Ages, and Petrographic Overview

Sample (Field Station)	Latitude N	Longitude W	Interpreted Age (Ma)	Petrography
		Late Deformational Intrusives: Granodiorite of Claraville		
1 (TC27)	35°13'06"	118°27'40"	90±2	weakly foliated, porphyritic biotite granodiorite
		Late Deformational Intrusives: Pegmatite Dike		
2 (CM620)	35°07'26"	118°44'21"	95+5/-1	nonfoliated pegmatitic garnet biotite granite
		Intrusive Suite of Bear Valley: Tonalite of Bear Valley Springs		
3 (BM684)	35°18'47"	118°39'23"	100±2	nonfoliated, porphyritic biotite tonalite
4 (TC15)	35°13'47"	118°29'29"	97+3/-0	foliated biotite hornblende tonalite
5 (TC42)	35°13'42"	118°29'46"	98+2/-1	foliated biotite hornblende tonalite
6 (TC40)	35°13'28"	118°28'58"	97+3/-0	foliated biotite hornblende tonalite
7 (CM25)	35°12'38"	118°39'47"	101+1/-2	foliated biotite hornblende tonalite
8 (CM26)	35°08'23"	118°37'03'	100±2	foliated biotite hornblende tonalite
9 (CM9)	35°02'27"	118°34'06"	100±2	strongly foliated biotite hornblende tonalite
10 (CM22b)	35°11'02"	118°38'45"	100±2	nonfoliated biotite hornblende quartz-diorite
		Intrusive Suite of Bear Valley: Hypersthene Tonalite of Bison Peak		
11 (TL197)	34°59'27"	118°32'16"	102+1/-2	foliated hypersthene hornblende biotite tonalite
		Intrusive Suite of Bear Valley: Metagabbro of Tunis Creek		
12 (WR84a)	34°58'59"	118°43'17"	102+1/-2	nonfoliated two-pyroxene hornblende gabbro (accessory metamorphic garnet)
13 (WR86)	34°58'27"	118°43'45"	102+1/-2	nonfoliated two-pyroxene hornblende gabbro (accessory metamorphic garnet)
14 (WR190)	34°58'40"	118°45'44"	n/d	nonfoliated olivine two-pyroxene hornblende gabbro (no zircon yield)
15 (PC227)	34°58'16"	118°46'42"	n/d	nonfoliated olivine two-pyroxene hornblende gabbro (no zircon yield)

TABLE 1. (continued)

Sample (Field Station)	Latitude N	Longitude W	Interpreted Age (Ma)	Petrography
		Gneiss Complex of the Tehachapi Mountains: Tonalite Gneiss of Tejon Creek		
16 (CM630)	35°07'30"	118°43'22"	115±10	biotite tonalite gneiss
17 (WR643)	35°01'28"	118°42'24"	117±4	hypersthene biotite tonalite gneiss
18 (WR171)	34°59'31"	118°43'44"	115±15	biotite hornblende tonalite layered gneiss
19 (WR30/2)	34°59'04"	118°43'29"	115±10	clinopyroxene hornblende quartz-diorite gneiss
20 (WR39)	34°56'38"	118°39'48"	113±4	clinopyroxene hornblende tonalite layered gneiss
		Gneiss Complex of the Tehachapi Mountains: Quartzofeldspathic Gneiss of Pastoria Creek		
21 (PC35)	34°55'10"	118°47'46"	110±15	biotite muscovite garnet granite gneiss (dike rock)
22 (PC31)	34°56'29"	118°49'32"	114±3	hornblende biotite granite gneiss
23 (PC32)	34°56'13"	118°49'08"	113±4	biotite granite gneiss
24 (PC34)	34°55'40"	118°48'04"	117±4	epidote biotite hornblende tonalite gneiss
25 (PC36)	34°54'59"	118°47'40"	112±3	epidote garnet biotite tonalite gneiss
26 (PC37)	34°54'30"	118°47'15"	115±3	biotite granite augen gneiss
27 (PC129)	34°55'31"	118°54'42"	115±3	garnet biotite tonalite
28 (WR91a)	34°57'30"	118°43"08"	113±5	garnet biotite leucotonalite gneiss
29 (WR40)	34°56'47"	118°40'41"	117±3	biotite granite augen gneiss
		Gneiss Complex of the Tehachapi Mountains: Augen Gneiss of Tweedy Creek		
30 (TC12a)	35°13'39"	118°29'18"	117±4	biotite granodiorite augen gneiss
		Gneiss Complex of the Tehachapi Mountains: Paragneiss of Comanche Point		
31 (CM110)	35°08'19"	118°46'53"	~1,460 (detritus)	strongly banded garnet graphite muscovite biotite quartzofeldspathic gneiss
		Kings Sequence Metasedimentary Framework Rock: Quartzite		
32 (CM640)	35°08'01"	118°33'46"	~1,708 (detritus)	two-feldspar garnet muscovite metaquartzite

dence provided here supporting the synplutonic nature of the deformation includes the age of the Mount Adelaide phase of the tonalite batholith (100±2 Ma, sample 3) which crosscuts the main internal fabric of the batholith, and a 95+5/-1 Ma date on a pegmatite dike swarm (sample 2) which crosscuts the gneissic banding in the Tejon Creek and Comanche Point units. The granodiorite of Claraville (90 Ma) also crosscuts high-temperature deformation fabrics in the tonalite of Bear Valley Springs and in its Kings sequence host.

The documentation of middle Cretaceous deep-crustal conditions within the study area carries important tectonic implications for the early Tertiary of southern California as well. As noted above, the crystalline rocks of the study area are overlain unconformably by Eocene marine strata. This implies a rapid latest Cretaceous to early Tertiary uplift and erosion event. Such an event may be related to the initial juxtaposition of the deep-level rocks with the Rand Schist. Similar schist bodies of the southern California region were tectonically emplaced during the same time interval [Haxel and Dillon, 1978; Ehlig, 1981; Silver et al., 1984].

Major questions in the petrotectonics of convergent plate junctures developed along continent edges concern the input of mantle or deep subduction zone-derived magma to the crust, and the interactions with preexisting crustal materials. The application of our geochronological and isotopic data to such questions is a main focus below.

U/Pb Zircon Age Data

U/Pb zircon age determinations were conducted on 30 samples from the crystalline rocks of the study area. Sample locations and petrographic data along with the interpreted ages are presented in Table 1. The isotopic data are presented in Table 2, along with notes on analytical procedures and uncertainties. The zircon samples were collected in order to perform specific tests on the age, petrogenesis, and structural evolution of the crystalline rocks. One of the first problems addressed was the possibility that remnants of Proterozoic crystalline rock occur within the gneiss complex of the Tehachapi Mountains. The zircon data, along with the map relations of the dated units, indicate that no such remnants exist in significant volume. This alone is considered to be an important contribution from the zircon data. Other questions considered in the zircon investigations include (1) age of the southernmost Sierran batholithic rocks, (2) age relations between such batholithic rocks and the gneiss complex, (3) the absolute chronology in the development of high-temperature deformation fabrics, and (4) the isotopic signature of detrital zircon in metasedimentary protoliths and the recognition of such zircon as contaminants within populations of adjacent igneous protoliths.

The zircon data are presented graphically in the form of $^{207}Pb/^{206}Pb$-$^{238}U/^{206}Pb$ concordia diagrams [after Tera and Wasserburg, 1972]. Internal concordance is used here to denote agreement of U-Pb and Pb-Pb ages of a given analysis within analytical uncertainty expressed graphically by the intersection of concordia with the error bars. External concordance is defined as agreement, or graphic overlap, in internally concordant ages from multiple fractions of a given sample or multiple samples from a given rock unit.

The zircon systematics presented here exhibit two distinct mechanisms in the production of discordant ages: (1) entrainment or inheritance of significantly older (Proterozoic) zircon in Cretaceous magmatic systems; and (2) open system loss of radiogenic Pb, with possible U gain, in response to Cretaceous high-temperature deep-crustal conditions. Several of the samples from the intrusive suite of Bear Valley and the sample from the granodiorite of Claraville exhibit the entrainment/inheritance mechanism. Samples from metasedimentary rocks exhibit the disturbance mechanism. Many of the samples from the gneiss complex display systematics interpreted as the result of minor inheritance followed by minor open system Pb loss and/or U gain. Our discussion will begin with sample suites for which the effects of the two mechanisms can be isolated.

Proterozoic Zircon in Cretaceous Magmatic Systems

The incorporation of Proterozoic zircon into Cretaceous magmatic systems plagues to various degrees all the major intrusive rocks studied. Our discussion will thus begin by characterizing the contaminant zircon and considering clear examples of such contamination. Zircon populations from two samples of the metasedimentary rocks (31 and 32) are dominated by Proterozoic grains. Figure 3a is a concordia plot which shows data from the paragneiss of Comanche Point (31) and a Kings sequence quartzite (32). The paragneiss array shows high dispersion with an upper intercept of 1,460±20 Ma and a lower intercept of 110±4 Ma (r factor = 0.9938 with r = 1 for perfect linear array). The upper intercept is interpreted as an approximate age of the detrital zircon within the psammitic protolith. The lower intercept corresponds in time with its partial melting at the time of the intrusion of the orthogneisses. Zircon homogeneity and a meager yield inhibited multiple fraction analysis of the quartzite population. The quartzite sample is from a septum encased within the tonalite of Bear Valley Springs (Figure 2). Its one data point is highly discordant with a $^{207}Pb/^{206}Pb$ age of 1,563 Ma. A chord passed through this point with a forced 100 Ma lower intercept (Bear Valley Springs age) yields a 1,708 Ma upper intercept. Detrital zircon ages of 1,800±100 Ma are common in the Kings sequence and also occur as a contaminant in spatially related Mesozoic igneous rocks [Saleeby, 1987; Saleeby et al., 1987]. Such a detrital zircon age is seen as an upper intercept in Figure 3b. Shown here are data from the granodiorite of Claraville (sample 1), a nondeformed pluton which was emplaced almost totally within Kings sequence quartzite (Figure 2). The sample 1 data show a highly discordant linear array with an upper intercept of 1,897+46/-47 Ma and a lower intercept of 90±1 Ma (r factor = 0.9964). The high linearity of the array in conjunction with the recognized upper intercept contaminant indicates that the lower intercept is the igneous age.

TABLE 2. U/Pb Zircon Age Data

Fraction[a] Properties	mg Sample	Concentrations ppm 238U	Concentrations ppm 206Pb*	Concentrations 206Pb/ 204Pb	Radiogenic Ratios 206Pb*/ 238U	Radiogenic Ratios 207Pb*/ 235U	Radiogenic Ratios 207Pb*/ 206Pb*	Isotopic Ages (Ma)[b] 206Pb*/ 238U	Isotopic Ages (Ma)[b] 207Pb*/ 235U	Isotopic Ages (Ma)[b] 207Pb*/ 206Pb*
Late Deformational Intrusives: Granodiorite of Claraville										
#1 biotite granodiorite										
165-120 μ	14.4	509	8.06	2,811	0.01828	0.1611	0.06396 (27)	116.8	151.7	740
10/20nm 120-80 μ	34.6	666	9.81	1,529	0.01701	0.1428	0.06094 (37)	108.7	135.7	637
80-45 μ	32.7	788	10.5	2,867	0.01533	0.1133	0.05322 (22)	98.1	109.0	338
<45 μ	26.6	967	12.0	1,830	0.01439	0.0984	0.04964 (26)	92.1	95.3	178
Late Deformational Intrusives: Pegmatite Dike										
#2 garnet biotite granite pegmatite dike										
1/20nm <165 μ	12.3	906	11.6	6,498	0.01475	0.0976	0.04801 (14)	94.4	94.6	99
Intrusive Suite of Bear Valley: Tonalite of Bear Valley Springs										
#3 biotite tonalite - Mount Adelaide phase										
80-45 μ	14.8	342	4.64	1,503	0.01564	0.1042	0.04832 (29)	100.1	100.6	114
2/20 <45 μ	7.0	350	4.71	2,458	0.01555	0.1032	0.04816 (26)	99.5	99.7	106
#4 biotite hornblende tonalite - eastern marginal phase										
120-80 μ	33.7	478	6.25	771	0.01509	0.1008	0.04850 (36)	96.6	97.6	123
2/20nm 80-45 μ	27.7	563	7.46	1,682	0.01531	0.1022	0.04847 (29)	98.0	98.9	122
#5 biotite hornblende tonalite - eastern marginal phase										
120-80 μ	45.7	379	5.11	2,200	0.01559	0.1036	0.04826 (24)	99.7	100.2	111
2/20nm 80-45 μ	28.2	463	6.22	2,607	0.01548	0.1034	0.04848 (23)	99.0	99.9	122
#6 biotite hornblende tonalite cupola - eastern marginal phase										
165-120 μ	32.0	248	3.43	604	0.01596	0.1125	0.05119 (38)	102.1	108.3	249
4/20nm 120-80 μ	13.8	305	4.20	690	0.01594	0.1140	0.05195 (37)	101.9	109.6	283
#7 biotite hornblende tonalite - main phase										
120-80 μ	21.2	858	11.8	4,440	0.01586	0.1054	0.04824 (17)	101.4	101.8	111
1/20nm 80-45 μ	23.2	830	11.4	2,284	0.01591	0.1061	0.04839 (24)	101.8	102.4	118
#8 biotite hornblende tonalite - main phase										
120-80 μ	17.1	567	7.63	1,432	0.01556	0.1022	0.04810 (29)	99.6	98.8	104
2/20nm 80-45 μ	22.9	675	9.12	1,555	0.01561	0.1032	0.04798 (28)	99.9	99.8	98
#9 biotite hornblende tonalite - main phase										
120-80 μ	30.5	593	8.02	2,796	0.01562	0.1043	0.04847 (20)	99.9	100.8	122
1/20nm 80-45 μ	29.4	635	8.50	4,686	0.01546	0.1021	0.04792 (16)	98.9	98.7	96
#10 quartz dioritic inclusion - main phase										
120-80 μ	24.1	624	8.46	3,852	0.01569	0.1041	0.04820 (17)	100.3	100.6	108
1/20nm 80-45 μ	22.2	710	9.70	6,166	0.01579	0.1049	0.04823 (14)	101.0	101.4	110

TABLE 2. (continued)

Fraction[a] Properties		mg Sample	Concentrations ppm 238U	Concentrations ppm 206Pb*	Concentrations 206Pb/ 204Pb	Radiogenic Ratios 206Pb*/ 238U	Radiogenic Ratios 207Pb*/ 235U	Radiogenic Ratios 207Pb*/ 206Pb*	Isotopic Ages (Ma)[b] 206Pb*/ 238U	Isotopic Ages (Ma)[b] 207Pb*/ 235U	Isotopic Ages (Ma)[b] 207Pb*/ 206Pb*
Intrusive Suite of Bear Valley: Hypersthene Tonalite of Bison Peak											
#11 hypersthene biotite hornblende tonalite											
	120-80 μ	22.4	296	4.07	4,567	0.01587	0.1050	0.04801 (15)	101.5	101.4	100
0/20nm	<80 μ	25.5	318	4.44	10,170	0.01613	0.1075	0.04838 (13)	103.1	103.7	118
Intrusive Suite of Bear Valley: Gabbroids of Tunis Creek											
#12 hornblende gabbro											
	165-120 μ	24.2	78.4	1.08	2,796	0.01585	0.1057	0.04813 (22)	101.4	102.0	106
1/20nm	120-80 μ	23.5	78.2	1.08	2,213	0.01594	0.1052	0.04814 (23)	102.0	101.6	106
	80-45 μ	12.3	75.6	1.06	2,998	0.01618	0.1090	0.04893 (20)	103.5	105.1	144
#13 hornblende gabbro											
	165-120 μ	25.6	64.3	.898	1,226	0.01613	0.1062	0.04781 (38)	103.2	102.6	90
2/20nm	120-80 μ	22.3	74.8	1.02	547.0	0.01579	0.1057	0.04767 (34)	101.0	102.1	98
	<80 μ	19.1	74.6	1.28	939.7	0.01982	0.1541	0.05642 (39)	126.5	145.5	469
Gneiss Complex of the Tehachapi Mountains: Tonalite Gneiss of Tejon Creek											
#16 biotite tonalite gneiss											
	165-120 μ	18.1	1,026	16.6	3,656	0.01867	0.1262	0.04907 (19)	119.3	120.7	151
1/20nm	165-120 μ	13.3	1,090	16.8	6,504	0.01781	0.1202	0.04900 (14)	113.8	115.3	147
	120-80 μ	19.6	989	15.3	11,220	0.01786	0.1212	0.04929 (12)	114.1	116.2	161
	<45 μ	16.8	1,019	16.1	11,190	0.01823	0.1248	0.04967 (12)	116.5	119.4	179
#17 biotite tonalite gneiss											
	165-120 μ	24.7	877	14.0	5,982	0.01840	0.1230	0.04852 (14)	117.5	117.8	124
1/20nm	<45 μ	18.1	979	15.5	7,329	0.01830	0.1225	0.04859 (12)	116.9	117.4	128
#18 biotite hornblende tonalite gneiss											
	165-120 μ	18.2	327	5.06	3,722	0.01788	0.1226	0.04979 (17)	114.2	117.5	185
1/20nm	120-80 μ	17.9	333	4.85	4,656	0.01684	0.1146	0.04940 (16)	107.7	110.2	166
	80-45 μ	16.7	375	5.65	4,269	0.01738	0.1182	0.04936 (16)	111.1	113.5	164
	<45 μ	11.0	248	3.83	5,196	0.01783	0.1247	0.05075 (20)	113.9	119.3	229
#19 hornblende quartz diorite											
	120-80 μ	12.8	217	3.55	2,074	0.01895	0.1293	0.05023 (25)	121.0	123.5	205
1/20nm	80-45 μ	11.8	227	3.62	2,142	0.01837	0.1266	0.05003 (25)	117.4	121.1	196
	<45 μ	4.4	232	3.73	875	0.01860	0.1292	0.04984 (36)	118.8	123.4	187
#20 hornblende tonalite gneiss											
	80-45 μ	27.7	169	2.59	5,475	0.01768	0.1178	0.04818 (14)	113.0	113.1	108
-1/20nm	<45 μ	5.1	202	3.08	4,087	0.01763	0.1189	0.04893 (15)	112.7	114.1	127

TABLE 2. (continued)

Fraction[a] Properties	mg Sample	Concentrations ppm 238U	Concentrations ppm 206Pb*	Concentrations 206Pb/ 204Pb	Radiogenic Ratios 206Pb*/ 238U	Radiogenic Ratios 207Pb*/ 235U	Radiogenic Ratios 207Pb*/ 206Pb*	Isotopic Ages (Ma)[b] 206Pb*/ 238U	Isotopic Ages (Ma)[b] 207Pb*/ 235U	Isotopic Ages (Ma)[b] 207Pb*/ 206Pb*
Gneiss Complex of the Tehachapi Mountains: Quartzofeldspathic Gneiss of Pastoria Creek										
#21 garnet granite gneiss (dike)										
120-80 μ	13.0	2,352	31.7	5,900	0.01559	0.1042	0.04852 (15)	99.7	100.7	124
2/20nm 80-45 μ	7.2	2,469	32.3	4,917	0.01514	0.1011	0.04850 (15)	96.9	97.9	123
#22 hornblende biotite granite gneiss										
120-80 μ	36.7	813	12.2	1,795	0.01729	0.1151	0.04831 (28)	110.5	110.6	114
2/20nm 80-45 μ	29.4	918	13.9	2,077	0.01754	0.1171	0.04845 (24)	112.1	112.5	121
#23 biotite granite gneiss										
120-80 μ	29.2	1,658	25.1	2,069	0.01748	0.1167	0.04848 (24)	111.7	112.2	122
2/20nm 80-45 μ	28.3	1,894	28.6	3,113	0.01747	0.1168	0.04851 (24)	111.6	112.3	124
<45 μ	6.8	1,825	28.0	1,869	0.01773	0.1173	0.04803 (34)	113.3	112.7	101
#24 biotite hornblende tonalite gneiss										
120-80 μ	33.0	222	3.49	3,885	0.01818	0.1221	0.04872 (18)	116.2	117.0	134
1/20nm 80-45 μ	30.2	338	5.36	7,455	0.01834	0.1239	0.04905 (12)	117.1	118.6	150
<45 μ	5.9	405	6.27	1,372	0.01787	0.1209	0.04909 (30)	114.2	115.9	152
#25 biotite tonalite gneiss										
120-80 μ	29.1	1,221	18.3	8,759	0.01731	0.1154	0.04837 (12)	110.6	110.9	118
1/20nm 80-45 μ	26.1	1,393	20.5	3,343	0.01704	0.1124	0.04817 (18)	108.9	108.2	105
#26 biotite granite augen gneiss										
120-80 μ	16.2	786	12.1	6,590	0.01781	0.1184	0.04827 (12)	113.8	113.7	113
1/20nm 80-45 μ	11.2	855	13.2	4,148	0.01786	0.1198	0.04858 (17)	114.1	114.9	127
#27 biotite garnet tonalite										
120-80 μ	14.6	335	5.24	1,348	0.01806	0.1212	0.04868 (30)	115.4	116.2	132
0/20nm 80-45 μ	13.8	343	5.28	2,820	0.01781	0.1184	0.04842 (20)	113.8	113.6	120
#28 garnet leucotonalite gneiss										
80-45 μ	24.5	763	11.6	5,071	0.01752	0.1164	0.04822 (14)	112.0	111.8	110
-1/20pm <45 μ	23.4	814	12.0	4,880	0.01701	0.1143	0.04876 (15)	108.8	109.9	136
#29 biotite granite augen gneiss										
120-80 μ	19.7	912	14.5	3,715	0.01836	0.1222	0.04834 (18)	117.3	117.1	116
1/20nm 80-45 μ	17.5	1,091	16.9	4,658	0.01791	0.1190	0.04818 (17)	114.6	114.2	108
Gneiss Complex of the Tehachapi Mountains: Augen Gneiss of Tweedy Creek										
#30 biotite granodiorite orthogneiss										
165-120 μ	15.1	897	13.8	3,374	0.01778	0.1191	0.04863 (19)	113.6	114.3	129
10/20nm 120-80 μ	8.7	1,022	15.6	2,227	0.01758	0.1184	0.04887 (25)	112.3	113.6	141
80-45 μ	22.8	1,132	17.0	3,465	0.01737	0.1156	0.04846 (19)	111.0	111.4	122
<45 μ	38.4	1,206	18.5	4,106	0.01774	0.1192	0.04879 (17)	113.4	114.4	137

TABLE 2. (continued)

Fraction[a] Properties	mg Sample	Concentrations ppm 238U	ppm 206Pb*	206Pb/ 204Pb	Radiogenic Ratios 206Pb*/ 238U	207Pb*/ 235U	207Pb*/ 206Pb*	Isotopic Ages (Ma)[b] 206Pb*/ 238U	207Pb*/ 235U	207Pb*/ 206Pb*
Gneiss Complex of the Tehachapi Mountains: Paragneiss of Comanche Point										
31 biotite quartzofeldspathic paragneiss										
165-120 μ	1.3	365	25.1	581	0.07946	0.9229	0.08428 (59)	493.0	664.0	1299
0/20pm 120-80 μ	8.7	633	26.1	2,778	0.04760	0.5165	0.07873 (31)	299.8	422.8	1165
80-45 μ	20.2	684	27.0	2,828	0.04558	0.4820	0.07675 (31)	287.4	399.5	1114
<45 μ	23.9	876	29.7	6,332	0.03916	0.4004	0.07420 (22)	247.6	342.0	1047
Kings Sequence Metasedimentary Framework Rock: Quartzite										
#32 impure quartzite										
-1/20pm <45 μ	25.0	512	38.0	1,999	0.08560	1.1420	0.09680 (44)	529.6	773.5	1563

a. Fractions separated by grain size and magnetic properties. Magnetic properties are given as nonmagnetic (nm) or paramagnetic (pm) split at side/front slopes for 1.7 amps on Frantz Isodynamic Separator. Samples hand-picked to >99% purity prior to dissolution. Dissolution and chemical extraction modified techniques after Krogh [1973].

b. The decay constants used for age calculations were $\lambda^{238}U = 1.55125 \times 10^{-10}$, $\lambda^{235}U = 9.8485 \times 10^{-10}$ [Jaffey et al., 1971]; $^{238}U/^{235}U(atom) = 137.88$. Common lead compositions used for nonradiogenic correction were based on blank and initial lead values, which were approximated from laboratory measurements and from feldspar determinations of nearby mid-Mesozoic granitoids [Chen and Tilton, 1978; Chen and Moore, 1982]. Common lead: $^{206}Pb/^{204}Pb = 18.8\pm0.1$, $^{207}Pb/^{204}Pb = 15.6\pm0.05$, $^{208}Pb/^{204}Pb = 37.7\pm0.2$. Analyses conducted at California Institute of Technology between 1981 and 1984, during which total blank averaged 0.1 ng Pb. Uncertainties are reported in last two figures (±) of radiogenic $^{207}Pb^*/^{206}Pb^*$ ratios based on agreement between spiked and unspiked aliquots, mass spectrometer statistics, and uncertainty in initial lead isotopic composition. Uncertainty in $^{206}Pb^*/^{238}U \simeq 0.8\%$ based on long-term reproducibility. Mass spectrometer performance monitored on a regular basis by runs of NBS SRM983 and 982 (Pb) and U500 (U) reference standards.

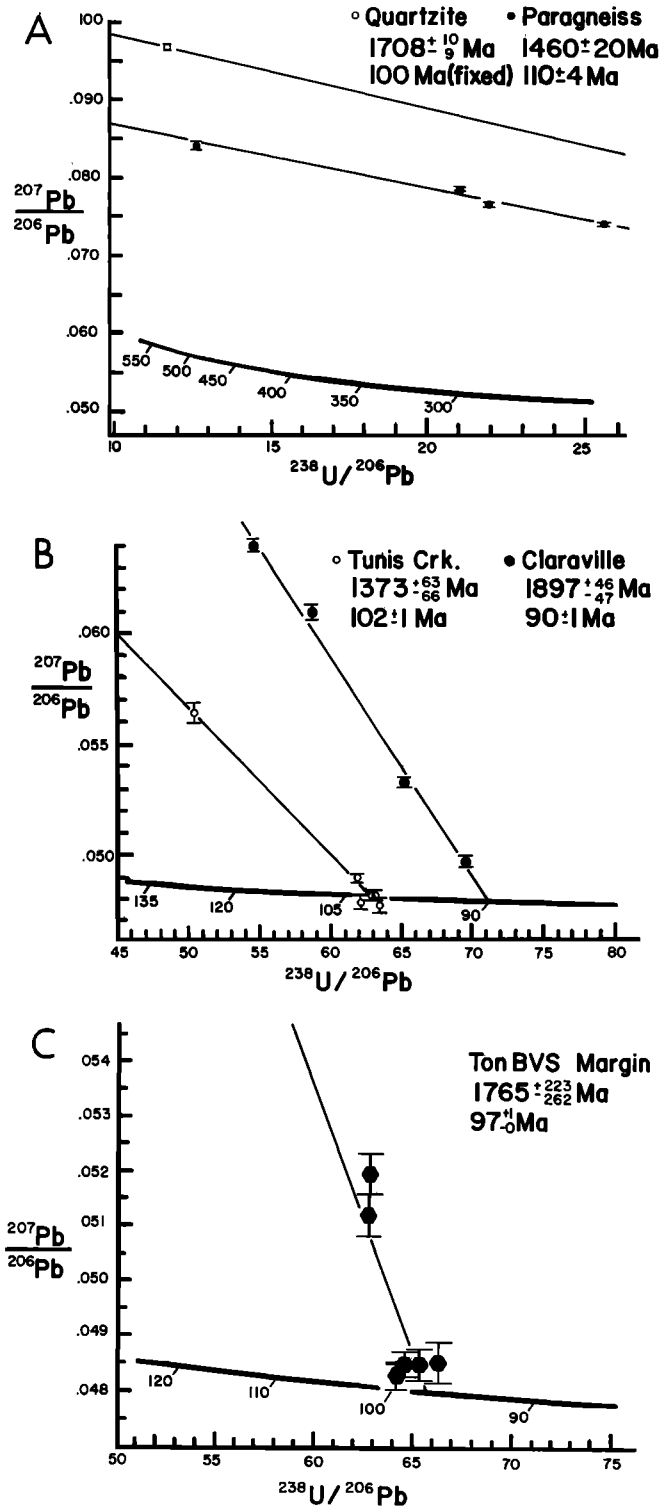

Fig. 3. Concordia diagrams [after Tera and Wasserburg, 1972] for (a) the Kings sequence quartzite (sample 32) and the paragneiss of Comanche Point (sample 31), both of the metasedimentary framework; (b) gabbroids of Tunis Creek (samples 12 and 13) and granodiorite of Claraville (sample 1); and (c) eastern marginal phases of the tonalite of Bear Valley Springs (samples 4, 5, and 6). Linear regression and errors in lower and upper intercepts are adapted from York [1969].

Gabbroic rocks of Tunis Creek have entrained small amounts of xenocrystic zircon with isotopic signatures similar to the paragneiss sample. The data points from samples 12 and 13 cluster around the 102 Ma lower intercept with most of them exhibiting external concordance. The fine fraction from each sample is dispersed up the discordia trajectory which yields an upper intercept of 1,373+63/-66 Ma (r factor = 0.9938). The U concentrations in the Tunis Creek zircon are quite low, ranging between 64 and 78 ppm (Table 2). Thus their systematics are highly susceptible to discordances induced by small amounts of older contaminant zircon. Contamination in the Tunis Creek samples is believed to have occurred at a relatively high structural level (entrainment during magmatic emplacement). This is suggested by the fact that only the fine fractions show the discordances, which is in reverse to what is commonly observed in populations with inheritance. For example, the Claraville zircon yields a well-dispersed discordia array with discordance increasing with grain size (Table 2). This is interpreted to reflect the incorporation of the contaminant zircon into the Claraville magma early in its history (inheritance) with sufficient time for substantial zircon overgrowth. In contrast, higher-level entrainment of contaminant grains results in shorter residence times, limited overgrowths, and poorer correlations with grain size. The Tunis Creek systematics are also consistent with the common observation that detrital zircon populations are dominated by finer grains (<60 μ) throughout much of the Sierran metamorphic framework [Saleeby, 1987]. This is reflected in zircon populations from samples 31 and 32 of this study.

The eastern marginal phase of the tonalite of Bear Valley Springs is variably contaminated with Proterozoic zircon. Figure 3c is a concordia plot of two samples from the eastern phase (4 and 5) and a nearby eastern phase cupola within the Kings sequence (sample 6). Samples 4 and 5 show minor discordance, and sample 6 is dispersed significantly up a discordia trajectory with an upper intercept of 1,765+223/-262 Ma and a lower intercept of 97+1/-0 Ma (r factor = 0.827). The relatively weak linear correlation arises from the dispersion of the lower data points along concordia. The dispersion may represent two distinct batches of magma (upper two and lower two data points), or minor open system behavior perhaps due to the location of these samples along a postbatholith shear zone. The upper intercept is typical of detrital zircon contaminants from the Kings sequence. The lower intercept corresponds to the igneous age of the tonalite batholith as discussed below.

Age of the Intrusive Suite of Bear Valley

Zircon systematics of samples from the Mount Adelaide and main phases of the tonalite of Bear Valley Springs and from the hypersthene tonalite of Bison Peak are summarized graphically in Figure 4a. This plot shows analogous segments of concordia and data points for a number of samples stacked above one another in order to facilitate comparisons between samples. There is a strong clustering of concordant ages around 100 Ma. In

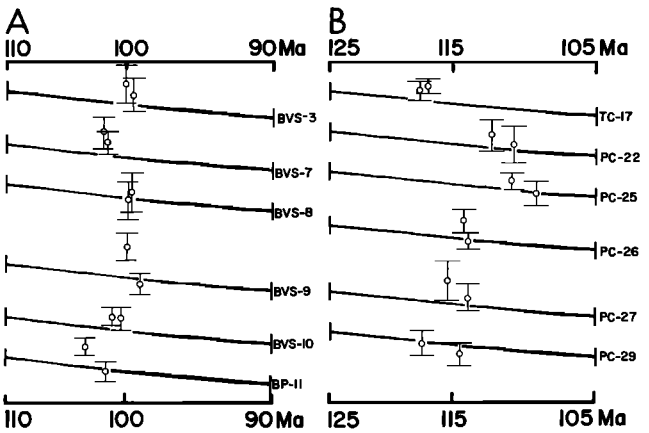

Fig. 4. Stacked segments of concordia and data points for selected samples of (a) the intrusive suite of Bear Valley and (b) the gneiss complex of the Tehachapi Mountains. These plots facilitate direct comparison between data points of the various samples and relations between error bars and concordia. Bars at ends of concordia segments show uncertainty in $^{207}Pb/^{206}Pb$ values of concordia from uncertainties in ^{238}U and ^{235}U decay constants [after Jaffey et al., 1971]. BVS, tonalite of Bear Valley Springs; BP, hypersthene tonalite of Bison Peak; TC, tonalite gneiss of Tejon Creek; PC, quartzofeldspathic gneiss of Pastoria Creek.

all cases where slightly discordant ages occur, dispersion mimics the inheritance/entrainment trajectories of the Figures 3b and 3c concordia diagrams. Furthermore, the internally concordant data points of Figures 4a, 3b, and 3c all fall within the ranges of the Tunis Creek and eastern margin Bear Valley Springs lower intercepts. These relations together clearly point to an igneous age of 100±3 Ma for the intrusive suite of Bear Valley.

The ±3 m.y. uncertainty in the age of the intrusive suite may encompass the emplacement of several distinct batches of magma. Specifically, the Tunis Creek and Bison Peak units may represent distinct batches emplaced 1-2 m.y. earlier than the main tonalite batholith. The Mount Adelaide phase of the batholith is clearly a young, distinct batch even though its externally concordant data points are in agreement with most of the other concordant points from the suite. The relatively nondeformed Mount Adelaide phase crosscuts synplutonic deformation fabrics in the main phase. Mafic inclusions within the batholith are interpreted as the remnants of synplutonic batches of mafic to quartz dioritic magma mixed into the main tonalite reservoir [Sams and Saleeby, 1987]. The zircon data on the sample 10 inclusion are consistent with this interpretation. Finally, the eastern marginal phase of the batholith may contain some of the youngest magma batches. This is suggested by the 97 Ma lower intercept given in Figure 3c. Internal contacts within the marginal phase are obscured by a zone of high ductile strain which follows the eastern phase and its bordering Kings sequence septa. The deformation zone cuts the eastern edge of the Mount Adelaide phase to the north of the study area and projects further northward towards a major Late Cretaceous shear zone mapped in the Lake Isabella region (Figure 1) [Saleeby and Busby-Spera, 1986].

In summary, the intrusive suite of Bear Valley was magmatically emplaced into a Kings sequence and gneiss complex host rock regime probably as several magma batches at 100±3 Ma. Many of the zircon ages are externally concordant within this age range, but some discordances arise from Proterozoic contaminants.

Age Constraints on Orthogneisses of the Tehachapi Mountains

Zircon data are presented for 15 orthogneiss samples which range in composition from quartz diorite to granite. Five are from the tonalite gneiss of Tejon Creek, and nine are from the quartzofeldspathic gneiss of Pastoria Creek. One additional sample (30) is from the granodioritic augen gneiss of Tweedy Creek, which is grouped into the gneiss complex on the basis of zircon systematics and structural relations with younger intrusives. The zircon systematics of 14 of the samples are grossly comparable, with variation within map units comparable to that observed between units. U/Pb ages cluster in the 110-120 Ma range, and most populations show moderate discordances. Examples of data sets including internally concordant ages are given in Figure 4b. Two types of discordances are exhibited. First there is dispersion off concordia similar to the subtle inheritance patterns noted in the data from the intrusive suite of Bear Valley (samples 17, 26, and 27). There is also

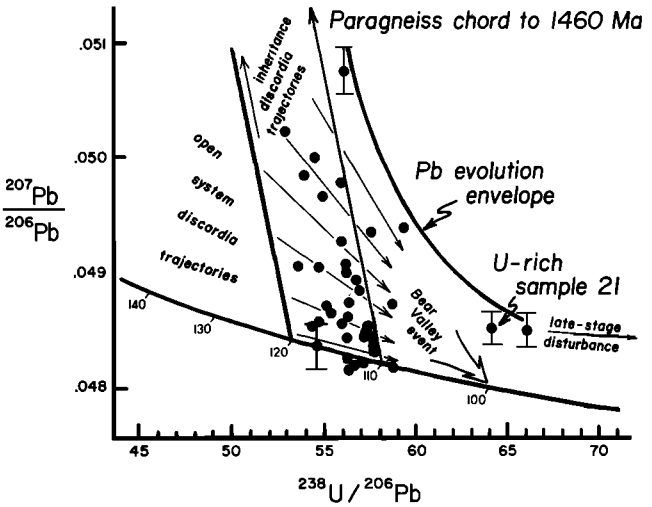

Fig. 5. Concordia diagram for all orthogneisses of the gneiss complex of the Tehachapi Mountains with paragneiss of Comanche Point reference chord (from Figure 3a). Representative uncertainties for data points are shown for four selected points by error bars. Pb-evolution envelope shows U-Pb isotopic systematics modeled as multistage evolution involving igneous crystallization at ~115 Ma with modest to no inheritance/entrainment of paragneiss zircon followed by limited open system behavior culminated during the Bear Valley suite intrusive event. Sample 21 shows evidence of additional late-stage open system behavior.

dispersion along concordia with the internally concordant data points (samples 22, 25, and 29). This pattern is generally not observed in the Bear Valley data and is interpreted to represent modest open system disturbance.

Figure 5 shows all of the orthogneiss data points plotted on a concordia diagram along with the paragneiss chord (Figure 3a) for reference. Typical ranges in error bars are shown for four representative data points. In general, the points show a scattering along the paragneiss chord with several internally concordant points dispersed along concordia between 117 and 108 Ma. This overall pattern is interpreted to have resulted from generally minor contamination by Proterozoic zircon in ~115 Ma magmatic systems, and then superimposed open system behavior. The open system behavior resulted from deep-crustal conditions within the Cretaceous batholithic belt (high amphibolite to granulite facies), and the related emplacement of the intrusive suite of Bear Valley. The ~115 Ma age derived for the igneous generation of the orthogneisses is consistent with a 117±5 Ma bulk rock Rb/Sr isochron determined on the zircon sample suite (Figure 6a, discussed below).

The Figure 5 data set defines a Pb-evolution envelope which encompasses inheritance and superimposed open system discordia trajectories that resulted in the observed Pb isotopic systematics. The inheritance trajectories are modeled after a paragneiss chord, and the open system trajectories are modeled after a 100 Ma (Bear Valley) culmination in the deep crustal magmatic-metamorphic environment. Later open system behavior is known to have affected one sample from the gneiss complex (21), as seen by displacement of the data points below the 100 Ma event. Such late-stage disturbance is considered to have been significant only in the U-rich (~2,500 ppm) sample 21. Age estimates for individual orthogneiss samples given in Table 1 and used for Sr_i calculations are based on the location of the respective data points within the envelope. The estimates cluster around 115 Ma.

A noteworthy aspect of the gneiss complex zircon data is the poor correlation between grain size, U concentration, and discordance. A general observation in igneous zircon populations is an increase in U concentration with decreasing grain size, and for disturbed populations, greater discordance with greater U concentration [Silver, 1962, 1964]. An example of the aberrant behavior of the gneiss complex zircon is shown in the sample 16 data, where U concentration and discordance are seen to be independent of grain size. To better understand the lack of the commonly observed relations, sample 16 was analyzed for intragrain distribution and intergrain homogeneity in U concentration by fission track radiography [Sams, 1986]. The fission tracks show strong inhomogeneity in U concentration, with no relations between grain size, zonation pattern, and overall track density (U concentration). Strongly zoned and cored grains dominate, and commonly three to four cycles in zonation are observed. Such zonation can be explained by variations in the conditions of zircon crystallization, and/or by the zircon population representing a polygenetic suite. In the first case, the tonalite could have existed at near-solidus conditions for an extended period of time at deep-crustal levels. In such an environment one might expect multiple cycles of zircon nucleation and crystallization, with varying influxes of uranium into the growing zircon. Variations in U concentration may be induced by crystal-melt partitioning during emplacement of multiple magma batches with varying compositions, or perhaps by the migration of metamorphic fluids during extended solidus and hot-subsolidus residence. Additional heterogeneities in U concentration were probably introduced by inheritance. The widespread zonation in U concentration suggests that recrystallization of the zircon did not occur. The U zonation patterns are interpreted to be consistent with a prolonged and complex history of igneous crystallization and hot subsolidus residence for the gneiss complex.

In summary, zircon populations from the orthogneisses exhibit concordant to moderately discordant age systematics with overall isotopic patterns suggestive of igneous crystallization at ~115 Ma. The discordances are interpreted to have resulted from a multistage evolution. Granitic to quartz dioritic magmas consumed minor amounts of Proterozoic zircon from partial to complete melts of metasedimentary framework material. The contaminant zircon was joined and ultimately isotopically dominated by new igneous zircon. Such igneous zircon grew over a possible extended period of time, or locally behaved as partial open systems in an extended hot subsolidus environment. This high-temperature environment culminated with the emplacement of the 100 Ma igneous suite of Bear Valley.

Strontium and Oxygen Isotopic Data

Bulk rock strontium and oxygen isotopic studies were performed on the zircon sample suite in conjunction with ongoing U.S. Geological Survey (Menlo Park) regional studies on geochemical variations within Mesozoic plutonic rocks. The Rb/Sr data are given in Table 3 and include three additional samples from the granodiorite of Claraville and 13 additional samples from the tonalite of Bear Valley Springs (locations shown in Figure 1). The Sr_i and O data reported here (Tables 3 and 4) are representative of the larger data set for the southernmost Sierra Nevada summarized by Ross [1983a,c]. Kistler and Peterman [1973, 1978] have noted a geographic variation in Sr_i measured on Mesozoic plutons, whereby a family of isopleths may be drawn along the major trend of the Sierra Nevada batholith. These workers noted that samples with $Sr_i > 0.706$ have field settings and petrochemical features suggestive of interaction with Proterozoic sialic materials, and those with $Sr_i < 0.706$ have seen little or no such interaction. The regional trend of the 0.706 isopleth is shown in Figure 1. Kistler and Peterman [1973, 1978] suggested that the 0.706 isopleth approximates the western edge of cryptic, largely magmatically remobilized, mid-Proterozoic crystalline basement. Neodymium and strontium isotopic studies on central Sierran batholithic rocks [DePaolo, 1981] suggest that such rocks east of the 0.706 isopleth attained their isotopic character by subequal mixtures of Cretaceous mantle-derived igneous material and Proterozoic sial-derived sedimentary material.

TABLE 3. Rubidium and Strontium Abundance and Isotopic Data

Sample* No.	Name	Rb, ppm	Sr, ppm	10,000/ Sr	Rb/Sr wt.	$^{87}Rb/^{86}Sr$ atom	$^{87}Sr/^{86}Sr$ Measured	$^{87}Sr/^{86}Sr$ Initial
			Late Deformational Intrusives: Granodiorite of Claraville					
1	TC27	71.2	562	17.79	0.127	0.367	0.70777	0.70731
A	DR4341	82.0	603	16.58	0.136	0.393	0.70850	0.70800
B	DR4102a	96.6	504	19.84	0.192	0.554	0.70817	0.70746
C	DR3737	86.0	893	11.20	0.096	0.279	0.70813	0.70777
			Late Deformational Intrusives: Pegmatite Dike					
2	CM620	91.2	61	164.20	1.498	4.332	0.71157	0.70576
			Intrusive Suite of Bear Valley: Tonalite of Bear Valley Springs					
3	BM684	19.6	455	21.98	0.043	0.125	0.70458	0.70440
4	TC15	18.5	360	27.78	0.051	0.148	0.70603	0.70583
5	TC42	30.8	341	29.33	0.090	0.261	0.70606	0.70570
6	TC40	48.1	578	17.30	0.083	0.241	0.70735	0.70703
7	CM25	55.9	399	25.06	0.140	0.405	0.70648	0.70591
8	CM26	69.2	392	25.51	0.177	0.512	0.70708	0.70637
9	CM9	104	388	25.77	0.268	0.775	0.70785	0.70677
10	CM22b	16.0	265	37.74	0.060	0.173	0.70629	0.70605
D	Sr14-73	55.0	347	28.82	0.159	0.46	0.70550	0.70485
E	Sr15-73	53.8	341	29.33	0.158	0.46	0.70600	0.70535
F	DR3427b	63.0	297	33.67	0.212	0.614	0.70649	0.70562
G	DR3575	85.5	346	28.90	0.247	0.715	0.70701	0.70599
H	DR3837	81.8	250	40.00	0.327	0.947	0.70725	0.70590
I	DR3670	63.2	313	31.95	0.202	0.584	0.70684	0.70601
J	DR3791	41.4	344	29.07	0.120	0.348	0.70546	0.70497
K	DR3858	72.6	285	35.09	0.255	0.737	0.70616	0.70511
L	DR4181	62.7	378	26.46	0.166	0.480	0.70493	0.70425
M	DR4184	53.8	323	30.96	0.167	0.481	0.70498	0.70430
N	DR4189	35.2	418	23.92	0.084	0.243	0.70483	0.70448
O	DR3631	57.8	640	15.63	0.090	0.261	0.70462	0.70425
P	DR3635	36.4	417	23.98	0.087	0.253	0.70479	0.70443
			Intrusive Suite of Bear Valley: Hypersthene Tonalite of Bison Peak					
11	TL197	36.6	330	30.30	0.111	0.321	0.70542	0.70496
			Intrusive Suite of Bear Valley: Gabbroids of Tunis Creek					
12	WR84	3.7	583	17.15	0.006	0.018	0.70502	0.70499
13	WR86	2.2	504	19.84	0.004	0.013	0.70506	0.70504
14	WR190	5.7	500	20.00	0.011	0.033	0.70504	0.70499
15	PC227	4.2	709	14.10	0.006	0.017	0.70495	0.70493
			Gneiss Complex of the Tehachapi Mountains: Tonalite Gneiss of Tejon Creek					
16	CM630	36.1	257	38.91	0.140	0.405	0.70534	0.70472
17	WR643	21.0	367	27.25	0.057	0.165	0.70545	0.70518
18	WR171	35.8	308	32.47	0.116	0.336	0.70518	0.70467
19	WR30/2	1.9	447	22.37	0.004	0.012	0.70480	0.70478
20	WR39	2.4	696	14.37	0.003	0.010	0.70501	0.70499
			Gneiss Complex of the Tehachapi Mountains: Quartzofeldspathic Gneiss of Pastoria Creek					
21	PC35	149	50	202.02	3.010	8.720	0.71965	0.70776
22	PC31	52.1	215	46.51	0.242	0.700	0.70627	0.70519
23	PC32	145	79	126.42	1.833	5.300	0.71336	0.70510
24	PC34	33.3	352	28.41	0.095	0.273	0.70511	0.70469
25	PC36	11.2	324	30.86	0.035	0.100	0.70515	0.70500
26	PC37	69.7	222	45.05	0.314	0.908	0.70613	0.70469
27	PC129	40.6	332	30.12	0.122	0.352	0.70650	0.70594
28	WR91a	18.7	353	28.33	0.053	0.153	0.70560	0.70536
29	WR40	56.7	138	72.46	0.411	1.180	0.70670	0.70480
			Gneiss Complex of the Tehachapi Mountains: Augen Gneiss of Tweedy Creek					
30	TC12a	66.7	216	46.30	0.309	0.890	0.70818	0.70682

TABLE 3. (continued)

Sample* No.	Name	Rb, ppm	Sr, ppm	10,000/ Sr	Rb/Sr wt.	$^{87}Rb/^{86}Sr$ atom	$^{87}Sr/^{86}Sr$ Measured	$^{87}Sr/^{86}Sr$ Initial
Gneiss Complex of the Tehachapi Mountains: Paragneiss of Comanche Point								
31	CM110	110	165	60.61	0.667	1.931	0.71442	0.71146
Kings Sequence Metasedimentary Framework Rock: Quartzite								
32	CM640	32.3	90.3	110.74	0.358	1.037	0.72581	0.72434

Rb and Sr concentrations were determined by x-ray energy dispersive techniques; uncertainties in the Rb/Sr values determined by this method are ±3% or less. Sr isotope ratios were measured with a 90°-sector, 46 cm mass spectrometer using double rhenium filament mode of ionization, and with automated data collection and reduction. Replicate analyses of the Eimer and Amend and NBS $SrCO_3$ standards yielded $^{87}Sr/^{86}Sr$ values of 0.70800± 0.00003 and 0.71023±0.00003, respectively. All Sr isotopic ratios are normalized to a $^{86}Sr/^{88}Sr$ value of 0.1194. Sr_i ratios were corrected for in situ ^{87}Rb decay by using U/Pb age determined for the sample, except for samples 14, 15, and lettered samples, where the age of the unit from other samples was used. For the metasedimentary units, the lower intercept was used for the paragneiss of Comanche Point (110 Ma), and the tonalite of Bear Valley Springs age (100 Ma) was used for the quartzite. Sr_i uncertainties ±0.00010.

* Samples 1-32 from Sams [1986]; A-C, F-O from Ross [1980, 1987] and Kistler and Ross [1987]; D-E from Kistler and Peterman [1978].

Isotopic and petrologic studies on mantle and crustal xenoliths [Domenick et al., 1983; Dodge et al., 1986] carried in late Cenozoic eruptives of the central Sierra are generally consistent with DePaolo's [1981] model, but with possible inclusion of additional components with isotopic characteristics bracketed by DePaolo's end-members. Reconnaissance O isotope data from Mesozoic plutonic rocks lying on the high side of the Sr_i = 0.706 isopleth in the southern Sierra show extensive interaction with metasedimentary material [Masi et al., 1981]. In a number of cases, $\delta^{18}O$ (SMOW) exceeds +10.0°/$_{oo}$, with the range of +6 to +10°/$_{oo}$ representing a normal range of igneous values and values of >+10°/$_{oo}$ representing sedimentary or highly contaminated igneous materials [Taylor, 1978]. Field, petrographic, and zircon data discussed above suggest that crystalline rocks of the southernmost Sierra Nevada were constructed from a mixture of Cretaceous mantle-derived gabbroic to tonalitic magma, and admixtures of partial to complete melts derived from metasedimentary framework rocks. Strontium and oxygen isotopic data presented below provide important constraints on such interpretations.

Strontium Isotopic Data

Initial $^{87}Sr/^{86}Sr$ values for all except the two metasedimentary samples (31 and 32) are calculated using the zircon ages summarized in Table 1. Sr_i for the orthogneisses and the intrusive suite of Bear Valley ranges from 0.70427 to 0.70677, except for the gneissic garnet granite dike (sample 21, Sr_i = 0.70776), which appears to be a highly contaminated and fractionated variant of the gneiss complex. The extent of contamination in the dike is discussed below with the fractionation being clearly exhibited by a Rb content of 149 ppm, a Rb/Sr ratio of 3.0, and a U concentration in zircon of ~2,500 ppm.

The gneiss complex of the Tehachapi Mountains yields a general bimodal suite of data, with the main orthogneisses clearly distinct from the paragneiss sample, and from the sample 21 dike. The tonalite gneiss of Tejon Creek has Rb/Sr < 0.12. Tonalites in the Pastoria Creek unit have Rb/Sr ratios of <0.1, while granites have a range of Rb/Sr ratios of 0.2 to 1.8. The low Sr_i and low Rb/Sr indicate that the orthogneisses probably had an upper mantle source, with the quartz diorite and tonalite gneisses representing relatively primitive magmas, while the granites in the Pastoria Creek unit represent differentiated magmas. A York [1969] regression of the orthogneiss data (Figure 6a), exclusive of the geographically separated samples 27 and 30, yields an isochron with an age of 116.7±5.4 Ma (2σ), with Sr_i = 0.70488±0.00019. As noted above, the isochron age is in close agreement with the zircon age constraints of the orthogneisses. The uncertainty in the Sr_i intercept in general encompasses the Sr_i values calculated for each sample based on the zircon ages. The well-defined isochron pattern of Figure 6a indicates a high degree of homogenization during the ~117 Ma igneous event. This is consistent with the paucity of restite observed within the orthogneisses, and the generally low values of metasedimentary contaminants modeled below with Sr and O isotopic data.

Figure 6b is a strontium evolution diagram for the Bison Peak and Tunis Creek samples of the intrusive suite of Bear Valley. The isochron age of 94.1±12.5 Ma (2σ) is within experimental error of the U/Pb zircon dates for these bodies. The Sr_i of 0.70499±0.00008 based on the intercept is also within the uncertainty of Sr_i values calculated for each sample from the zircon ages. This Sr_i value is substantially elevated relative to similar Cretaceous batholith-related gabbroids which intrude the Kings-Kaweah ophiolite belt to the north [Saleeby and Chen, 1978]. Likewise the

TABLE 4. Oxygen Isotopic Data for Igneous Rocks of the Study Area and Simple Mixing Models Based on Oxygen and Strontium Isotopic Compositions and Concentrations

Sample*	$\delta^{18}O$‰ (SMOW)†	% Metased 5.7/ 18.3	% Metased 8.5/ 18.3	INITIAL $^{87}/^{86}Sr$	% Metasedimentary 0.7034/ 0.7243	% Metasedimentary 0.7034/ 0.7115	% Metasedimentary 0.7047/ 0.7243	% Metasedimentary 0.7047/ 0.7115	% M.S. Multi-constrained
Late Deformational Intrusives: Kings Sequence Metasedimentary Framework									
1 gr	11.3	42	27	0.70731	18	48	13	39	18-27?
2 gr	10.0	32	14	0.70776	20	54	16	46	16-20
Tonalite of Bear Valley Springs: Kings Sequence Metasedimentary Framework									
4 tn	10.1	29	14	0.70583	11	29	6	17	11-14?
5 tn	9.1	22	5	0.70570	11	28	5	15	5-11
6 tn	10.1	29	14	0.70703	17	44	12	35	12-14
7 tn	8.6	19	1	0.70591	12	30	6	18	6-12
8 tn	9.6	26	9	0.70637	14	36	9	25	9-14
9 tn	9.1	22	5	0.70677	16	41	11	31	11-16
10 dr	7.8	14	<0	0.70605	12	32	7	20	7-12
Hypersthene Tonalite of Bison Peak: Paragneiss Metasedimentary Framework									
11 tn	5.7	0	<0	0.70496	7	18	2	4	0?
Gabbroid of Tunis Creek: Paragneiss Metasedimentary Framework									
12 gb	7.2	9	<0	0.70499	7	19	2	5	5- 9
13 gb	8.1	15	<0	0.70504	7	19	2	5	5-15
14 gb	7.6	12	<0	0.70499	7	19	2	5	5-12
15 gb	8.6	18	1	0.70493	7	18	1	4	4-18
Tonalite Gneiss of Tejon Creek: Paragneiss Metasedimentary Framework									
16 tn	10.1	29	13	0.70472	6	15	0	1	13-15
17 tn	10.5	32	17	0.70518	8	21	3	8	17-21
18 tn	6.8	7	<0	0.70467	6	15	0	0	0- 7
19 dr	8.5	18	0	0.70478	6	16	1	2	2-16
20 tn	8.4	18	<0	0.70499	7	19	2	5	5-18
Quartzofeldspathic Gneiss of Pastoria Creek: Paragneiss Metasedimentary Framework									
21 gr	10.0	32	14	0.70776	20	54	16	45	32-45?
22 gr	9.3	27	8	0.70519	8	21	3	8	8-21
23 gr	10.9	38	23	0.70510	8	20	2	6	20-23
24 tn	8.6	19	1	0.70469	6	15	0	0	1-15
25 tn	9.5	25	8	0.70500	7	19	2	5	8-19
26 gr	9.4	27	9	0.70469	6	15	0	0	9-15
27 tn	10.3	30	15	0.70594	12	31	7	19	15-19
28 tn	8.7	20	2	0.70536	9	23	4	10	10-20
29 gr	10.7	37	21	0.70480	6	16	1	2	16-21
Augen Gneiss of Tweedy Creek: Kings Sequence Metasedimentary Framework									
30 gr	10.8	38	21	0.70682	16	42	11	32	16-21?
Paragneiss of Comanche Point									
31	18.3			0.71146 at 110 Ma					
Quartzite, Kings Sequence									
32	17.4			0.72434 at 100 Ma					

Two-component mixing model for relative masses of rock based on Sr and O isotopic compositions (as indicated) and concentrations. End-member compositions are after $\delta^{18}O$ = +5.7 [Taylor, 1978; this study] or +8.5 [Fleck and Criss, 1985], and +18.3 (this study); Sr_i = 0.7034 [Saleeby and Chen, 1978] or 0.7047, and 0.7243 or 0.7115 (this study). Sr concentrations used given in Table 3. O concentration using 85% SiO_2 for metasediments based on regional patterns in Kings sequence impure quartzite/psammite modes in comparison with Pettijohn [1963]. O concentrations in various igneous rocks based on chemical data of Ross [1987] and J.B. Saleeby and B. Chappell (unpublished data, 1983). The multiconstrained model is based on overlap between O and Sr models and using Sr values only for indicated framework rocks. Question marks denote no overlap with intermediate values between differing models shown.

* gr, granitic; tn, tonalitic; dr, dioritic; gb, gabbroic.

† Oxygen was extracted using a ClF_3 method and was reacted with hot graphite to yield CO_2 for mass spectrometric analysis. The isotopic data are reported in the conventional $\delta^{18}O$ notation, where $\delta^{18}O$ is the relative difference in isotopic ratio between a sample and SMOW (Standard Mean Ocean Water), expressed in parts per thousand (‰). Replicate analyses indicate a typical precision of ±0.20‰.

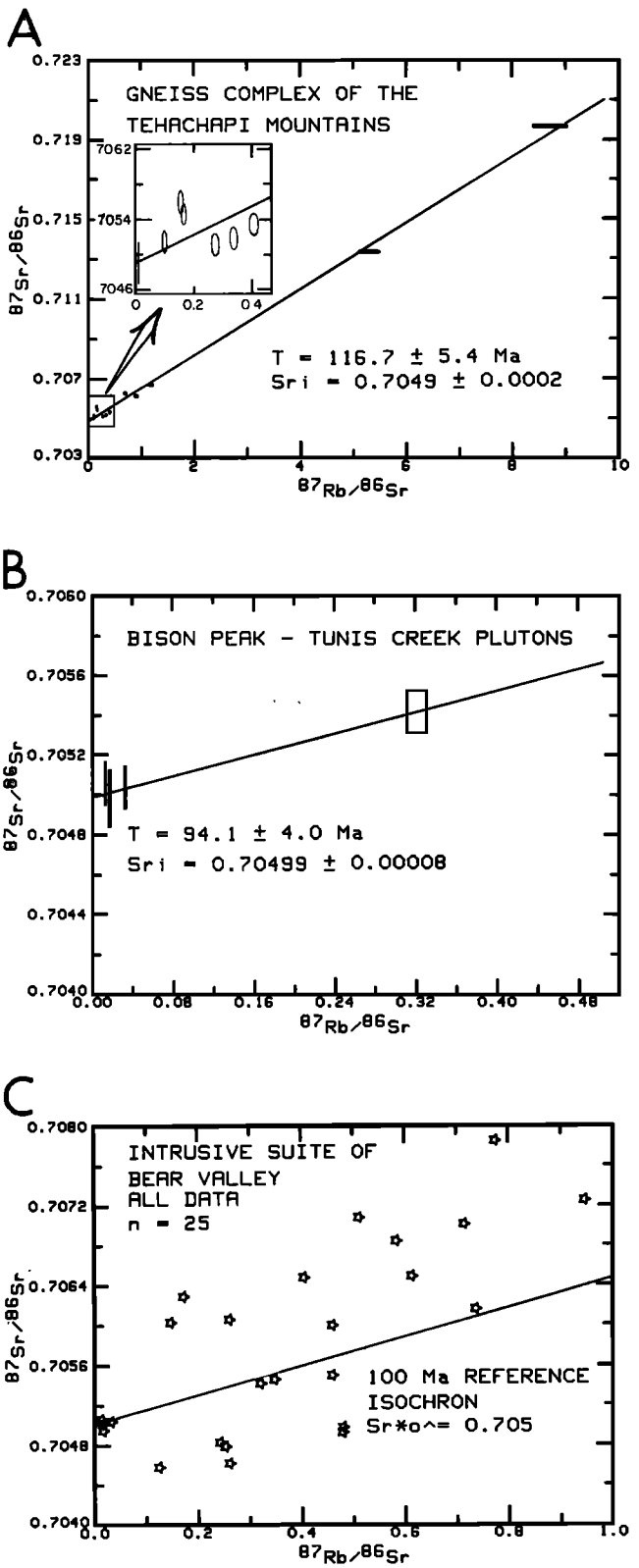

Fig. 6. Strontium evolution diagrams for (a) gneiss complex of Tehachapi Mountains exclusive of samples 27 and 30; (b) Bison Peak-Tunis Creek units of intrusive suite of Bear Valley (samples 11-15); and (c) the tonalite of Bear Valley Springs (all data points of Table 3) with a 100 Ma reference isochron based on zircon age. Uncertainties for (a) and (b) isochrons are at 1-σ.

mafic inclusion from the main phase of the batholith (sample 10) has an elevated Sr_i (0.70605) which is comparable to nearby main phase tonalite host rocks. These isotopic patterns indicate that mafic members of the intrusive suite were contaminated with crustal materials, which is also demonstrated in the zircon systematics. The low Rb contents (<6 ppm) and Rb/Sr values (≤0.01) for the Tunis Creek samples (Table 3) are consistent with the observation of cumulate textures in the gabbros.

In contrast to Figure 6b, a strontium evolution diagram (Figure 6c) for the tonalite of Bear Valley Springs shows extreme scatter about a 100 Ma isochron. Sr_i for these specimens at 100 Ma ranges from 0.70425 to 0.70677. This is the largest variation in Sr_i presently reported for a Cordilleran batholithic pluton. There is a geographic pattern to the variation in Sr_i. Samples to the northwest of the White Wolf-Breckenridge fault system, including the Mount Adelaide phase (Figure 2), have the lowest Sr_i in the entire study area (0.70425±0.00010). Main and eastern border phase samples south of the fault system as well as the mafic inclusion exhibit the higher Sr_i values. The magnitude of variation in Sr_i can be due to an inhomogeneous source material for the parent magma of the batholith, magma mixing from multiple sources, or contamination of the magma by metasedimentary materials. The latter mechanism is known to have at least locally operated by the zircon discordance patterns.

Strontium data on the two metasedimentary samples are quite different. The paragneiss of Comanche Point (sample 31) yields $^{87}Sr/^{86}Sr$ of 0.71146 at 110 Ma, its lower zircon intercept or migmatization age. The quartzite (sample 32) yields $^{87}Sr/^{86}Sr$ of 0.72434 at 100 Ma, the age of its peak metamorphism. The $^{87}Sr/^{86}Sr$ ratios were calculated in order to display the isotopic compositions at the time of the major igneous and mixing events under consideration. The large differences in $^{87}Sr/^{86}Sr$ in conjunction with the Rb/Sr ratios (Table 3), and the widely differing detrital zircon ages, indicate distinctly different source terranes. As noted above, however, the quartzite and paragneiss protoliths may have originated as part of the same stratigraphic sequence or facies system, and both carry strong Proterozoic sialic provenance imprints.

A plot of Sr_i versus 10,000/Sr for specimens of the intrusive suite of Bear Valley, the paragneiss, and the quartzite shows a general positive correlation (Figure 7a). Faure et al. [1974] showed that this type of correlation was compatible with simple mixing of two isotopically and compositionally distinct end-members. In the case represented by Figure 7a, either or both the quartzite and paragneiss could be the low strontium concentration-high $^{87}Sr/^{86}Sr$ end-member, whereas the least radiogenic specimens of the intrusive suite could approximate the high strontium concentration-low $^{87}Sr/^{86}Sr$ end-member. An expanded view of the intrusive suite data (Figure 7b) indicates that the suite is composed of three principal magma types and that crystal fractionation was important in addition to assimilation. The first magma type (diamonds), with the lowest Sr_i of ~0.7042, is made up of the tonalite of Bear Valley Springs (Mount Adelaide and main phases) northwest of the White Wolf-

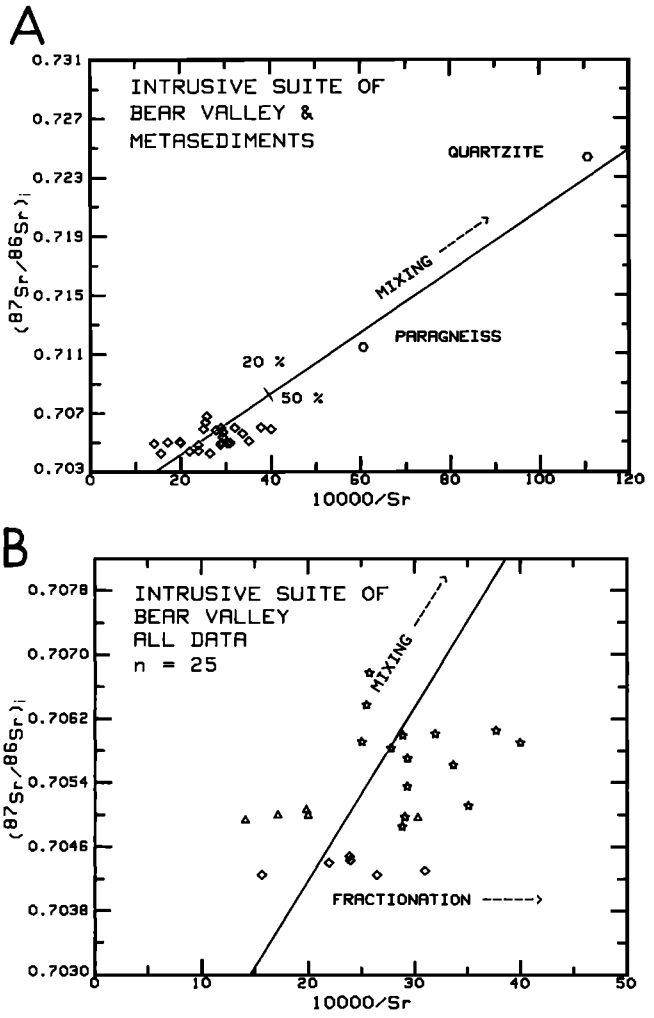

Fig. 7. (a) Plot of Sr_i versus 10,000/Sr for specimens of the intrusive suite of Bear Valley, paragneiss of Comanche Point, and Kings sequence quartzite. The 20% and 50% marks represent admixtures of quartzite and paragneiss respectively, along hypothetical mixing line. (b) Expanded view of the intrusive suite data points and suggested mechanisms for isotopic composition and concentration variations. Diamonds, samples northwest of White Wolf-Breckenridge fault; triangles, Bison Peak and Tunis Creek units and mixed Bear Valley Springs phase; stars, main and eastern marginal phases of batholith southeast of White Wolf-Breckenridge fault.

Breckenridge fault system. The second (triangles), with an intermediate Sr_i of ~0.7049, is made up of the hypersthene tonalite of Bison Peak, the gabbroids of Tunis Creek, and the mixed phases of the tonalite of Bear Valley Springs. Sr concentration trends within these two groups can be explained primarily by crystal fractionation, although it is not clear how many batches of magma are represented in the data and at what stage they attained their Sr_i values. The third magma type is composed of the main and eastern phases of the tonalite of Bear Valley Springs southeast of the White Wolf-Breckenridge fault system. Sr_i is mostly about 0.7059, but ranges as high as 0.70677. The Rb/Sr systematics of this type are suggested to represent both crystal fractionation and substantial assimilation of metasedimentary material.

Oxygen Isotopes and Simple Mixing Models

Oxygen isotopic data for the zircon samples are presented as $\delta^{18}O$ (SMOW) in Table 4. Masi et al. [1981] presented a regional synthesis of oxygen isotopic data for the Sierra Nevada batholith, and Ross [1983c] summarized these and additional new data for the area southwest of Mineral King (Figure 1). These data in general show that plutons emplaced into the Kings sequence framework are enriched in ^{18}O, suggesting contamination by the metasedimentary material. Samples 1, 4, 6, and 30, which include the Claraville pluton, the eastern border phase of the tonalite of Bear Valley Springs, and the augen gneiss of Tweedy Creek, show such an enrichment pattern. Most of the intrusive suite of Bear Valley, however, yields $\delta^{18}O$ values of less than +9.6°/$_{oo}$, and as low as +5.7°/$_{oo}$ (Bison Peak), suggesting a subordinate or a lack of metasedimentary components. Samples from the gneiss complex yield $\delta^{18}O$ values suggestive of little to considerable contamination (+6.8 to +10.9°/$_{oo}$). The metasedimentary protoliths of samples 31 and 32 are further demonstrated by $\delta^{18}O$ values of +18.3 and +17.4°/$_{oo}$.

The Bison Peak $\delta^{18}O$ value of +5.7°/$_{oo}$ and the paragneiss value of +18.3°/$_{oo}$ are used as end-member components in a simple mixing model summarized in Table 4 [after Sams, 1986]. The tabulated data show the mass percentage of metasedimentary material necessary to alter the isotopic compositions of low $\delta^{18}O$ magmas to obtain the observed values. This model permits 14-29% contamination of the tonalite of Bear Valley Springs, 9-18% for the gabbroids of Tunis Creek, 7-29% for the tonalite gneiss of Tejon Creek, and 19-45% for the quartzofeldspathic gneiss of Pastoria Creek. An alternative model is shown in Table 3, where the incorporation of sedimentary components or hydrothermally altered oceanic crust into the mantle source region is assumed to have altered the mantle isotopic signature, yielding a $\delta^{18}O$ value of +8.5°/$_{oo}$ prior to crustal contamination [Fleck and Criss, 1985]. In this model, the tonalite of Bear Valley Springs is generally less than 10% contaminated, the gabbroids of Tunis Creek are noncontaminated, and samples from the gneiss complex are either noncontaminated or up to 23% contaminated.

The $\delta^{18}O$ value determined for the Bison Peak sample demonstrates that at least some tonalitic magmas rose to the current level of exposure with preservation of pristine mantle compositions. This is supported by a number of significantly negative values in the second model. Furthermore, the contamination of the Tunis Creek zircon population with grains bearing a Proterozoic isotopic signature indicates some level of metasedimentary contamination for the gabbroids. Thus the second model does not appear totally applicable. However, with the first model, rocks of tonalitic composition show up to 38% contamination, which is inconsistent with bulk compositions. Thus variable noncontaminated initial values between +5.7 and +8.5°/$_{oo}$ seem to be re-

quired. The mixing relations can be further constrained by incorporating the Sr data.

Data are also tabulated for simple mixing models based on Sr isotopic compositions and concentrations (Table 3). A Sr_i value of 0.7034 [Saleeby and Chen, 1978] was used for the non-contaminated mantle composition in the first set of models. This mantle value is based on data from Cretaceous calcic-gabbro intrusives, similar to those of the Tunis Creek unit, but emplaced into the Paleozoic Kings-Kaweah ophiolite to the north of the study area (Figure 1) [Saleeby and Sharp, 1980]. Contaminant $^{87}Sr/^{86}Sr$ end-member values of 0.72434 (quartzite at 100 Ma) and 0.71146 (paragneiss at 110 Ma) are used in the first two models. These models, as well as the next set, show that 2-3 times as much paragneiss is needed as a contaminant compared to the quartzite in order to yield the observed results. In the second set of models, the minimum Sr_i from the gneiss complex (0.70467) is used as the non-contaminated value. This value is intended to represent a possible Sr isotopic signature acquired from a third cryptic component in the mixing system. Such a component could be lower crustal materials beneath the Kings sequence framework, or crustal materials introduced into the mantle source regime by subduction. This second set of models show that significantly less contamination from the metasedimentary framework rocks is required if a more radiogenic Sr_i was carried into the area of contamination by the initial magmas.

A multiconstrained range of metasedimentary contamination values is also shown in Table 3. These values are based on the overlap observed in the Sr and O models, and by use of the Sr mixing values obtained on the observed metamorphic framework rocks (quartzite versus paragneiss). This can also be demonstrated by plotting Sr_i versus $\delta^{18}O$ (Figure 8) with the quartzite and paragneiss $\delta^{18}O$ and $^{87}Sr/^{86}Sr$ values at 100 Ma and 110 Ma plotted as well. The distribution of data points appears to reflect the field settings of the samples. The eastern sector of the cluster of points consists almost entirely of samples emplaced into Kings sequence quartzitic framework rocks. This sector trends along a hyperbolic trajectory which projects towards the quartzite data point. The western sector consists of samples emplaced into or to the west of the paragneiss. This sector trends towards the paragneiss data point. The relations shown in Figure 8 suggest that plutonic rocks northeast of the Tejon Creek area (Figure 2) were perhaps contaminated preferentially by quartzitic rocks, whereas those to the southwest, including the NW trending belt of tonalitic gneiss of Tejon Creek, were contaminated by the paragneiss. Such relations are consistent with the inheritance patterns observed in the zircon data as well. Inherited and detrital zircon in the Claraville intrusion, eastern phase of the tonalite of Bear Valley Springs, and quartzite (samples 1, 4, 5, 6, and 32) carry isotopic signatures of 1,700-1,900 Ma. In contrast, the paragneiss and Tunis Creek samples (31, 12, and 13) carry signatures of 1,370-1,460 Ma, and the more discordant orthogneiss data points cluster along the paragneiss chord. Thus in the multiconstrained model, rocks in the eastern sector are constrained to attain a

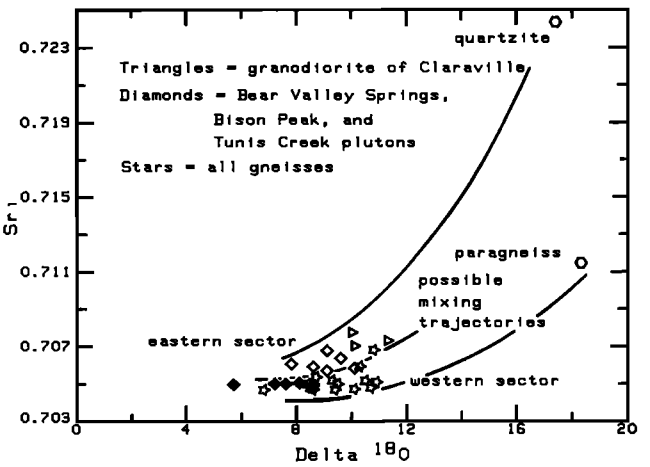

Fig. 8. Plot of initial $^{87}Sr/^{86}Sr$ versus $\delta^{18}O$ with points showing geographic grouping into data cluster sectors apparently trending towards spatially related metasedimentary samples. Solid diamonds are Bison Peak and Tunis Creek units which were emplaced into the paragneiss framework.

contaminant Sr signature similar to that of the quartzite, while those in the western sector attain a signature similar to that of the paragneiss. It is difficult to assess the possible effect of crystal fractionation on the mixing patterns shown in Figure 8, since plagioclase, hornblende, and pyroxene are all observed as cumulate phases in gabbroic-tonalitic suites of the study area as well as in western Sierra batholithic rocks to the north [Saleeby and Sharp, 1980; Sams and Saleeby, 1987]. Relative fractionation of these phases will have markedly different effects on the $\delta^{18}O$ versus Sr_i trajectories [see DePaolo, 1981].

A number of interesting points emerge from the multiconstrained model. (1) Many samples appear to have entered the level of framework contamination with Sr_i and $\delta^{18}O$ values already elevated above pristine mantle values. This argues for a possible third significant component as mentioned above. (2) There is significant overlap in the values for granitic versus tonalitic rocks of the gneiss complex, although tonalitic and dioritic members do occupy the lower end of the spectrum. This further suggests that fractionation was working in conjunction with assimilation to yield the lithologic variation observed in the orthogneisses. An extreme example of this is the sample 21 gneissic dike which shows strong evidence of being highly fractionated as discussed above as well as having the highest modeled value of metasedimentary contamination (up to 45%). (3) The majority of metasedimentary contaminant values are below 20%, which is substantially below the general Nd-Sr mixing model presented by DePaolo [1981]. The lower values are likely to be typical of the more western zones of the composite batholith. This is also suggested within DePaolo's data set. (4) A comparison of the results for the intrusive suite of Bear Valley samples in the multiconstrained model (Table 3) with the Figure 7a mixing model (based on Sr content and Sr_i) shows nearly complete overlap.

The mechanism for mixing of the metasedimentary components into the magmatic systems is not clear. In general, restite is absent. Lenses of metaquartzite and marble within the igneous rocks represent the main refractory phases of the Kings sequence. Regional metamorphic patterns in Kings sequence rocks indicate that psammitic and the more impure quartzitic protoliths preferentially undergo anatexis as the deeper levels to the south are approached [Saleeby et al., 1986; Saleeby and Busby-Spera, 1986]. We suggest that such psammitic materials in the study area were in most cases completely melted and contributed to the magmatic systems. Such melting and mixing may have occurred at a deeper level. However, the myriad of mafic inclusions within many of the igneous rocks attest to a dynamic environment where magmas of differing compositions mixed. Within such an environment the proximal melt products of the metasedimentary framework rocks may be grossly homogenized into the magma systems. In this regard the highly deformed quartzite/marble septa shown in Figure 2 may be thought of as large restite lenses.

Conclusions

1. The distinctive orthogneisses of the southernmost Sierra Nevada are predominantly Early Cretaceous (~115 Ma) in age; thus, direct remnants of Proterozoic sialic basement are probably not exposed in the Sierra Nevada.

2. Since the gneisses represent the deepest exposed levels of the Cretaceous Sierra Nevada batholithic belt [Saleeby et al., 1986; Sams and Saleeby, 1987], they offer important information on the structure and petrogenesis of sialic crust by Cordilleran-type batholithic magmatism. The majority of the magmas were extracted from the mantle by subduction-related magmatism in the Cretaceous.

3. The Cretaceous orthogneiss magma batches were intruded into a continent-derived early Mesozoic metasedimentary framework. The metasedimentary rocks are known to have sat at least locally on oceanic crust. Models calling on continental basement for such prebatholithic strata based on high Sr_i (>0.706) values measured on enclosing plutons are poorly constrained, since the isotopic patterns can be equally satisfied by magmatic assimilation of continent-derived sedimentary materials.

4. Some of the orthogneiss magmas assimilated up to 20% of their mass in completely melted metasedimentary framework material, and the mixture was highly homogenized.

5. The thermal-magmatic culmination of the gneiss complex is represented by a 100±3 Ma tonalitic batholith and smaller gabbroic to tonalitic plutons intruded into the complex.

6. Intense ductile deformation related to deep crustal magmatism and metamorphism ceased between 95 and 100 Ma.

7. The zircon U/Pb systematics of the orthogneisses and batholithic intrusives record mainly system closure during magmatic crystallization. Some zircon systems exhibit discordances resulting from limited open system behavior during extended deep batholithic residency, and/or from scattered inheritance/entrainment of Proterozoic detrital zircon derived from metasedimentary admixtures.

8. The Sr and O isotopic data clearly identify both mantle-derived magmatic and sialic detrital components as end-members and admixtures in the igneous and metamorphic rocks of the study area. Subtleties in the isotopic data call for a possible third component which may have been lower-level ensimatic accretionary material or subducted oceanic crust. Sr and Rb concentration data indicate that crystal fractionation operated in conjunction with assimilation.

The age data presented in this study also provide important data for the study of the upper crust of the Sierran batholithic belt. The central Sierra Nevada offers exposures of silicic volcanic rocks and caldera remnants, with ages similar to the deep-level rocks of the study area [Tobisch et al., 1986; Saleeby et al., 1986, 1987]. Along a regional traverse between the deep-level and volcanic rocks, numerous mesozonal plutons of similar age are intruded into the Kings sequence framework, which southward increases in overall metamorphic grade and textural reconstitution. Thus, the southern half of the range offers an oblique section through upper batholithic crust of a rather narrow age range (~20 m.y.). Rapid growth of such young crust was driven by subduction-related mantle magmatism, which, by fractionation and crustal assimilation, produced voluminuous silicic plutons and volcanic rocks.

Acknowledgments. Field and zircon geochronological work was supported by NSF grants EAR 8018811, EAR 8218460, and EAR 8419731 awarded to Saleeby. Fieldwork by Sams was also supported by Geological Society of America Penrose grants. Special thanks to the Tejon Ranch Company for access to much of the study area. Discussions with D.C. Ross, John Sharry, L.T. Silver, A.L. Albee, and H.P. Taylor, Jr., have been very helpful. Reviews by G.L. Farmer, R.J. Fleck, J.M. Mattinson, and J. Wooden were of great assistance. California Institute of Technology Division of Geological and Planetary Sciences contribution 4467.

References

Chen, J.H., and J.G. Moore, Uranium-lead isotopic ages from the Sierra Nevada batholith, J. Geophys. Res, 87, 4761-4784, 1982.

Chen, J.H., and G.T. Tilton, Lead and strontium isotopic studies of the southern Sierra Nevada batholith, California, Geol. Soc. Am. Abstr. Programs, 10, 99-100, 1978.

DePaolo, D.J., A neodymium and strontium isotopic study of the Mesozoic calc-alkaline granitic batholiths of the Sierra Nevada and Peninsular ranges, California, J. Geophys. Res., 86, 10,470-10,488, 1981.

Dodge, F.C.W., L.C. Calk, and R.W. Kistler, Lower crustal xenoliths, Chinese Peak lava flow, central Sierra Nevada, J. Petrol., 27, 1277-1304, 1986.

Domenick, M.A., R.W. Kistler, F.C.W. Dodge, and M. Tatsumoto, Nd and Sr isotopic study of crustal and mantle inclusions from the Sierra Nevada and implications for batholith petrogenesis, Geol. Soc. Am. Bull., 94, 713-719, 1983.

Ehlig, P.L., Origin and tectonic history of the basement terrane of the San Gabriel Mountains,

central Transverse Ranges, in The Geotectonic Development of California, W.G. Ernst, ed., pp. 253-283, Prentice-Hall, Englewood Cliffs, N.J., 1981.

Elan, R., High grade contact metamorphism at the Lake Isabella north shore roof pendant, southern Sierra Nevada, California, Ph.D. thesis, 202 pp., Univ. So. Calif., Los Angeles, 1985.

Faure, G., J.R. Bowman, D.H. Elliot, and L.M. Jones, Strontium isotope composition and petrogenesis of the Kirkpatrick basalt, Queen Alexandra Range, Antarctica, Contrib. Mineral. Petrol., 48, 153-169, 1974.

Fleck, R.J., and R.E. Criss, Strontium and oxygen isotopic variations in Mesozoic and Tertiary plutons in central Idaho, Contrib. Mineral. Petrol., 90, 291-308, 1985.

Green, T.H., Anatexis of mafic crust and high pressure crystallization of andesite, in Orogenic Andesites and Related Rocks, R.S. Thorpe, ed., pp. 465-487, John Wiley, New York, 1982.

Harris, P.B., Geology of the Tunis Creek-Pastoria Creek area, Kern County, Calif. Div. Mines Geol. Bull., 170, Map Sheet 2, 1954.

Haxel, G.B., and J. Dillon, The Pelona-Orocopia schist and Vincent-Chocolate Mountain thrust system, southern California, Pac. Coast Paleogeogr. Symp., 2, D.G. Howell, ed., Soc. Econ. Paleont. and Mineral., 453-469, 1978.

Jaffey, A.H., K.F. Flynn, L.E. Glendenin, W.C. Bentley, and A.M. Essling, Precision measurement of half-lives and specific activities of ^{235}U and ^{238}U, Phys. Rev. C, 4, 1889-1906, 1971.

Kistler, R.W., and Z.E. Peterman, Variations in Sr, Rb, K, Na and initial $^{87}Rb/^{86}Sr$ in Mesozoic granitic rocks and intruded wall rocks in central California, Geol. Soc. Am. Bull., 84, 3489-3512, 1973.

Kistler, R.W., and Z.E. Peterman, Reconstruction of crustal blocks of California on the basis of initial strontium isotopic compositions of Mesozoic granitic rocks, U.S. Geol. Surv. Prof. Pap. 1071, 17 pp., 1978.

Kistler, R.W., and D.C. Ross, Strontium isotopic systematics of plutons in the Sierra Nevada south of latitude 36° N, U.S. Geol. Surv. Bull., in press, 1987.

Krogh, T.E., A low-contamination method for hydrothermal decomposition of zircon and extraction of U and Pb for isotopic age determinations, Geochim. Cosmochim. Acta, 37, 485-494, 1973.

Masi, U., J.R. O'Neil, and R.W. Kistler, Stable isotope systematics in Mesozoic granites of central and northern California and southwestern Oregon, Contrib. Mineral. Petrol., 76, 116-126, 1981.

Nilsen, T.H., and S.H. Clarke, Jr., Sedimentation and tectonics in the early Tertiary continental borderland of central California, U.S. Geol. Surv. Prof. Pap. 925, 64 pp., 1975.

Pettijohn, F.J., Data of geochemistry, chap. 5, Chemical composition of sandstones--Excluding carbonate and volcanic sands, U.S. Geol. Surv. Prof. Pap. 440-S, 21 pp., 1963.

Ross, D.C., Reconnaissance geologic map of the southernmost Sierra Nevada (north to 35° 30' N), U.S. Geol. Surv. Open File Rep. 80-307, 22 pp., 1980.

Ross, D.C., Generalized geologic map of the southern Sierra Nevada, California, showing the location for which K-Ar radiometric age data and Rb/Sr data have been determined, U.S. Geol. Surv. Open File Rep. 83-231, 1 sheet, scale 1:250,000, 1983a.

Ross, D.C., Petrographic (thin section) notes on selected samples from hornblende-rich metamorphic terranes in the southernmost Sierra Nevada, California, U.S. Geol. Surv. Open File Rep. 83-587, 36 pp., 1983b.

Ross, D.C., Generalized geologic map of the southern Sierra Nevada, California, showing the location of basement samples for which whole rock ^{18}O has been determined, U.S. Geol. Surv. Open File Rep. 83-904, 1983c.

Ross, D.C., Mafic gneissic complex (batholithic root?) in the southernmost Sierra Nevada, California, Geology, 13, 288-291, 1985.

Ross, D.C., The metamorphic and plutonic rocks of the southernmost Sierra Nevada, California, and their tectonic framework, U.S. Geol. Surv. Prof. Pap., in press, 1987.

Saleeby, J.B., Ocean floor accretion and volcanoplutonic arc evolution of the Mesozoic Sierra Nevada, in The Geotectonic Development of California, W.G. Ernst, ed., pp. 132-181, Prentice-Hall, Englewood Cliffs, N.J., 1981.

Saleeby, J.B., Discordance patterns in Pb/U zircon ages of the Sierra Nevada and Klamath Mountains, Geol. Soc. Am. Abst. Programs, 19-6, in press, 1987.

Saleeby, J.B., and C.J. Busby-Spera, Fieldtrip guide to the metamorphic framework rocks of the Lake Isabella area, southern Sierra Nevada, California, in Mesozoic and Cenozoic Structural Evolution of Selected Areas, East-Central California, G.C. Dunne, ed., pp. 81-94, Geological Society of America, Boulder, Co., 1986.

Saleeby, J.B., and J.H. Chen, Preliminary report on initial lead and strontium isotopes from ophiolitic and batholithic rocks, southwestern foothills Sierra Nevada, California, U.S. Geol. Surv. Open File Rep. 78-701, 375-376, 1978.

Saleeby, J.B., and W.D. Sharp, Chronology of the structural and petrologic development of the southwest Sierra Nevada foothills, California, Geol. Soc. Am. Bull., 91-II, 1416-1535, 1980.

Saleeby, J.B., S.E. Goodin, W.D. Sharp, and C.J. Busby, Early Mesozoic paleotectonic-paleogeographic reconstruction of the southern Sierra Nevada region, Pac. Coast Paleogeogr. Symp., 2, D.G. Howell, ed., 311-336, 1978.

Saleeby, J.B., D.B. Sams, and O.T. Tobisch, A down-plunge view of the Sierra Nevada batholith: from resurgent caldera to ultrametamorphic levels, Geol. Soc. Am. Abstr. Programs, 18, 179, 1986.

Saleeby, J.B., R.W. Kistler, S. Longiaru, J.G. Moore, and W.J. Nokelberg, Middle Cretaceous metavolcanic sequences preserved in the Central Sierra Nevada batholith, California, in Cordilleran Magmatism, J.L. Anderson, ed., Geological Society of America, Boulder, Co., in press, 1987.

Sams, D.B., U/Pb zircon geochronology, petrology, and structural geology of the crystalline rocks of the southernmost Sierra Nevada and Tehachapi Mountains, Kern County, California, Ph.D. thesis, 315 pp., Calif. Inst. of Technol., Pasadena, 1986.

Sams, D.B., and J.B. Saleeby, Geology and petrotectonic significance of the crystalline rocks of the southernmost Sierra Nevada, California, in Rubey Volume VII, W.G. Ernst, ed., Prentice-Hall, Englewood Cliffs, N.J., in press, 1987.

Sams, D.B., J.B. Saleeby, D.C. Ross, and R.W. Kistler, Cretaceous igneous, metamorphic and deformational events of the southernmost Sierra Nevada, California, Geol. Soc. Am. Abstr. Programs, 15, 294, 1983.

Sharry, J., The geology of the western Tehachapi Mountains, California, Ph.D. thesis, 215 pp., Mass. Inst. of Technol., Cambridge, 1981.

Silver, L.T., Older Precambrian geochronology in Cochise County, southeastern Arizona, J. Geophys. Res., 67, 1657, 1962.

Silver, L.T., The relationship between radioactivity and discordance in zircons, Nuclear Geophysics, 1075, Nuc. Sci. Ser. Rep. 38, pp. 34-39, Natl. Academy of Sci., Natl. Res. Council, Washington, D.C., 1964.

Silver, L.T., D.B. Sams, M.I. Bursik, R.W. Graymer, J.A. Nourse, M.A. Richards, and S.L. Salyards, Some observations on the tectonic history of the Rand Mountains, Mojave Desert, California, Geol. Soc. Am. Abstr. Programs, 16, 333, 1984.

Taylor, H.P., Jr., Oxygen and hydrogen isotopic studies of plutonic granitic rocks, Earth Planet. Sci. Lett., 38, 177-210, 1978.

Tera, F., and G.J. Wasserburg, U-Pb systematics in lunar basalts, Earth Planet. Sci. Lett., 17, 65-78, 1972.

Tobisch, O.T., J.B. Saleeby, and R.S. Fiske, Structural history of continental volcanic arc rocks, eastern Sierra Nevada, California: A case for extensional tectonics, Tectonics, 5, 65-94, 1986.

Yeats, R.S., Quaternary flake tectonics of the California Transverse Ranges, Geology, 9, 16-20, 1981.

York, D., Least-squares fitting of a straight line with correlated errors, Earth Planet. Sci. Lett., 5, 320-324, 1969.

Zen, E., Implications of magmatic epidote-bearing plutons on crustal evolution in the accreted terranes of northwestern North America, Geology, 13, 266-269, 1985.

Zen, E., and J.N. Hammarstrom, Magmatic epidote and its petrologic significance, Geology, 12, 515-518, 1984.

R. W. Kistler, U.S. Geological Survey,345 Middlefield Road, Menlo Park, CA 94025.

J. B. Saleeby and D. B. Sams, Division of Geological and Planetary Sciences, California Institute of Technology, 170-25, Pasadena, CA 91125.

(Received September 12, 1986;
revised April 22, 1987;
accepted April 30, 1987)